80 V, 3.5 kW BLDC motor driver inverter

REF_80VDC_3.5KW_OPE2

About this document

Scope and purpose

This document describes the functionalities of the REF_80VDC_3.5KW_OPE2 motor drive board for 80 V battery-powered brushless DC (BLDC) motor drives operating with trapezoidal or sensorless field-oriented control (FOC) as used in applications such as outdoor power equipment up to 3.5 kW. This system solution is based on the PSOC™ C3 series microcontroller (MCU) operating with Infineon floating point firmware and 120 V OptiMOS™ 6 TOLT top-side cooled power MOSFETs.

Intended audience

This document addresses the market for high power 80 V battery-powered motor drive applications, aimed at designers wishing to provide a high-performance system solution as well as reduce system costs; also design engineers, applications engineers, and students.

Infineon components featured

- PSC3M5EDAFQ1 (Arm® Cortex® M33 32-bit MCU+FPU+DSP, 180 MHz, 128 kB flash, 64 kB SRAM, E-LQFP-80)
- IPTC017N12NM6 (OptiMOS™ 6 120 V/1.7 mΩ PG-HDSOP-16-U01 TOLT)
- IPT039N15N5 (OptiMOS™ 5 150 V/3.9 mΩ PG-HSOF-8 TOLL)
- 2ED2182S06F (650 V high-side and low-side gate driver IC, PG-DSO-8)
- 1EDL8011 (135 V high-side disconnect switch gate driver IC, PG-DSO-8)

Table of contents

1 Introduction

1.1 Outdoor power equipment

Outdoor power equipment (OPE) refers to high power construction and gardening tools such as lawn mowers, leaf blowers, hedge trimmers, and chainsaws. Motor drive systems in OPE are typically required to deliver power in the 3 to 5 kW power range. Older gasoline-powered outdoor power equipments are typically bulky, heavy, noisy, and produces CO^2 emissions. With new laws and environmental regulations being passed, this type of equipment is gradually being replaced with cordless battery-powered alternatives. 72-80 V lithium-ion battery packs are well suited for these applications as a tradeoff between lower current and safer voltage.

The need for smaller, safer, cordless, and more sustainable devices challenges the industry to optimize thermal management, battery runtime, and EMI, while handling weight and size constrains.

There are three main challenges in designing battery-powered OPE:

1. The first is maximizing energy output while keeping the motor drive as small and light as possible. OPE motor drives must offer efficient performance at sufficient power to support the torque and speed requirements
2. The second is thermal management and minimization of heat produced by electrical power conversion, which also wastes battery power. Therefore, the motor drive needs to operate with the highest possible efficiency to minimize bulky and heavy heat sinks
3. The third is safety. The OPE needs to include protection against possible faults and safe shutdown to avoid potential fire hazard and injury to the user

These challenges, alongside factors like robustness, reliability, and adherence to EMI standards impose constraints the motor drive must fulfill. Infineon’s latest power products can tackle these design challenges and help achieve system optimization.

Battery powered OPE is based on BLDC or PMS motors, which are commutated by controlled switching of the inverter instead of using mechanical brushes. Windings are energized in a determined sequence to generate a rotating magnetic field. The rotor permanent magnet attempts to align with the stator field, producing torque and rotary motion. As with mechanical commutation, electronic commutation helps achieve unidirectional torque similar to a conventional DC machine. In BLDC or PMS motors, the rotor consists of permanent magnets, while the stator is wound with a specific number of poles. Rotor position can be sensed using digital Hall effect sensors embedded into the stator, or sensorless control algorithms can be used to determine the position and speed from the phase currents.

1.2 REF_80VDC_3.5KW_OPE2 motor drive board

This document describes Infineon's REF_80VDC_3.5KW_OPE2 system solution reference board optimized for 80 V battery-powered tools operating with sensorless field-oriented control. The current design embodies the electrical driving system for PMSM and BLDC machines with sensorless operation or with Hall sensors. The default control method is sensorless FOC, however with alternative firmware trapezoidal or vector operation with Hall sensors is also supported.

The control method implements a vector speed-control algorithm based on the BLDC motor using pulse-width modulation (PWM) and three current shunts for phase current measurement.

The firmware is from Infineon's motor control firmware solution suite developed using the floating point PSOC™-C3 Arm® Cortex® M33 MCU.

With this reference board, you can evaluate the OPE motor drive system solution using the control capabilities of the MCU by means of the implemented control algorithm. The board includes a switch for changing the motor direction and a speed control potentiometer.

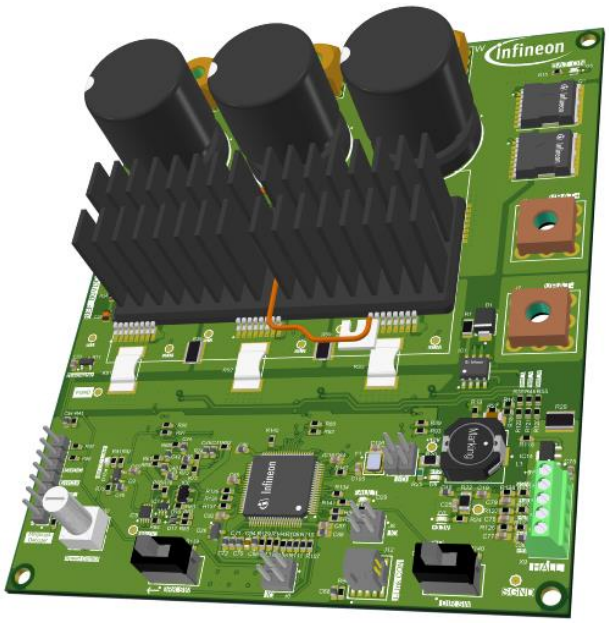

Figure 1 The REF_80VDC_3.5KW_OPE2 reference board

Introduction

The REF_80VDC_3.5KW_OPE2 board system block diagram of the main system is as follows:

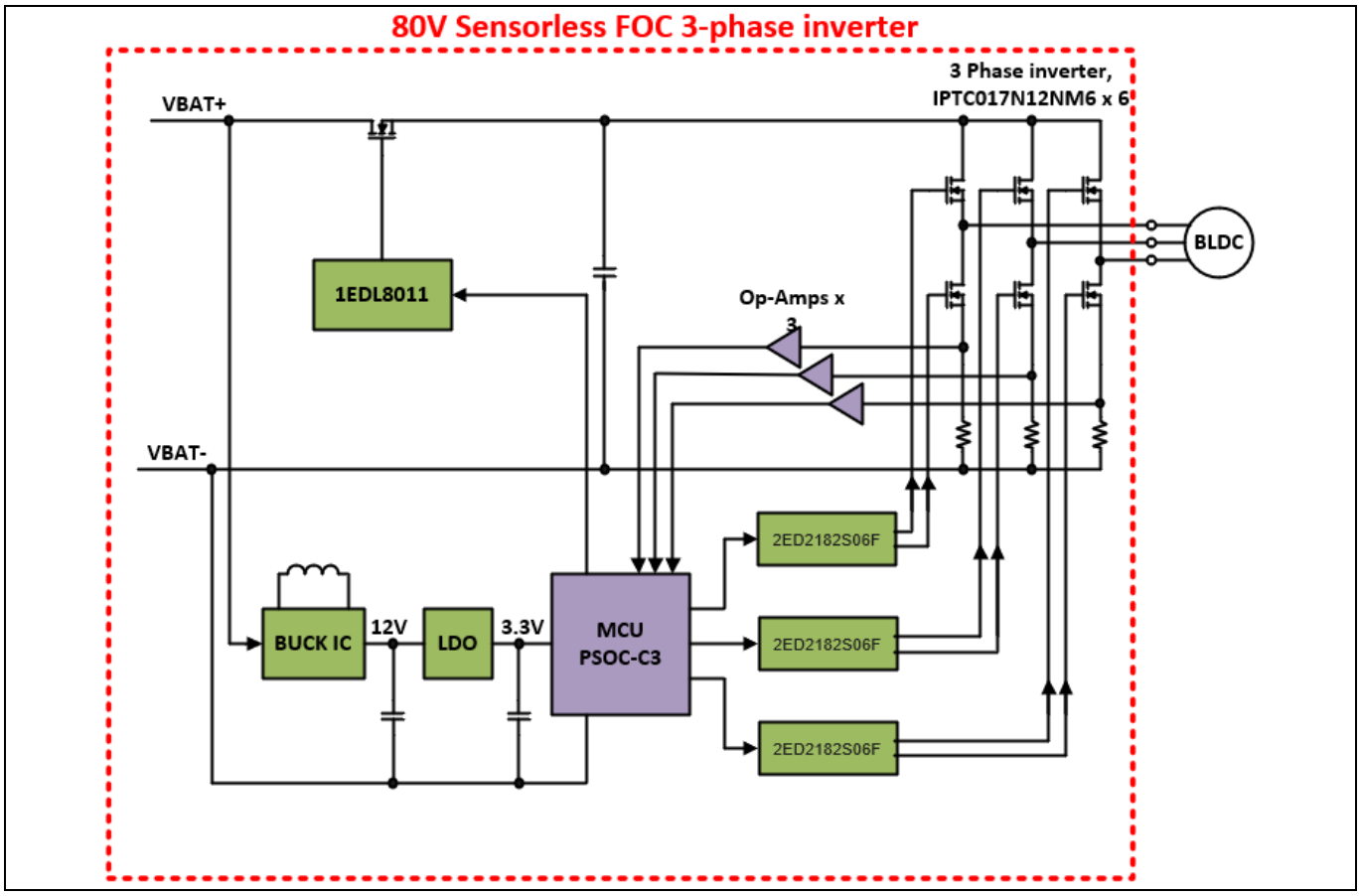

Figure 2 Simplified system block diagram

2 Specifications

Input and output in normal operation:

- DC input voltage 60-80 V, nominal 72 V
- Maximum input current 50 ADC
- Output voltage three-phase trapezoidal and sensorless FOC control
- Maximum output current per phase 55 A_{rms}
- Maximum output power 3500 W for not more than a minute
- Maximum continuous output power 2600 W

Control scheme:

- Supports Trapezoidal commutation with Hall sensors and sensorless FOC
- Switching frequency 15 kHz
- Three current shunts

Protection features:

- Input overcurrent
- Phase output overcurrent
- Thermal shutdown

Maximum component temperature:

In an ambient temperature of 30°C, the maximum allowed component temperatures are:

- Resistors less than 100°C
- Ceramic capacitors, film capacitors, and electrolytic capacitors less than 100°C
- MOSFET transistors and diodes less than 100°C
- ICs less than 100°C

Dimensions of evaluation board:

- Maximum width 4.0 inches/102.98 mm
- Maximum length 5.0 inches/125 mm

3 Schematics

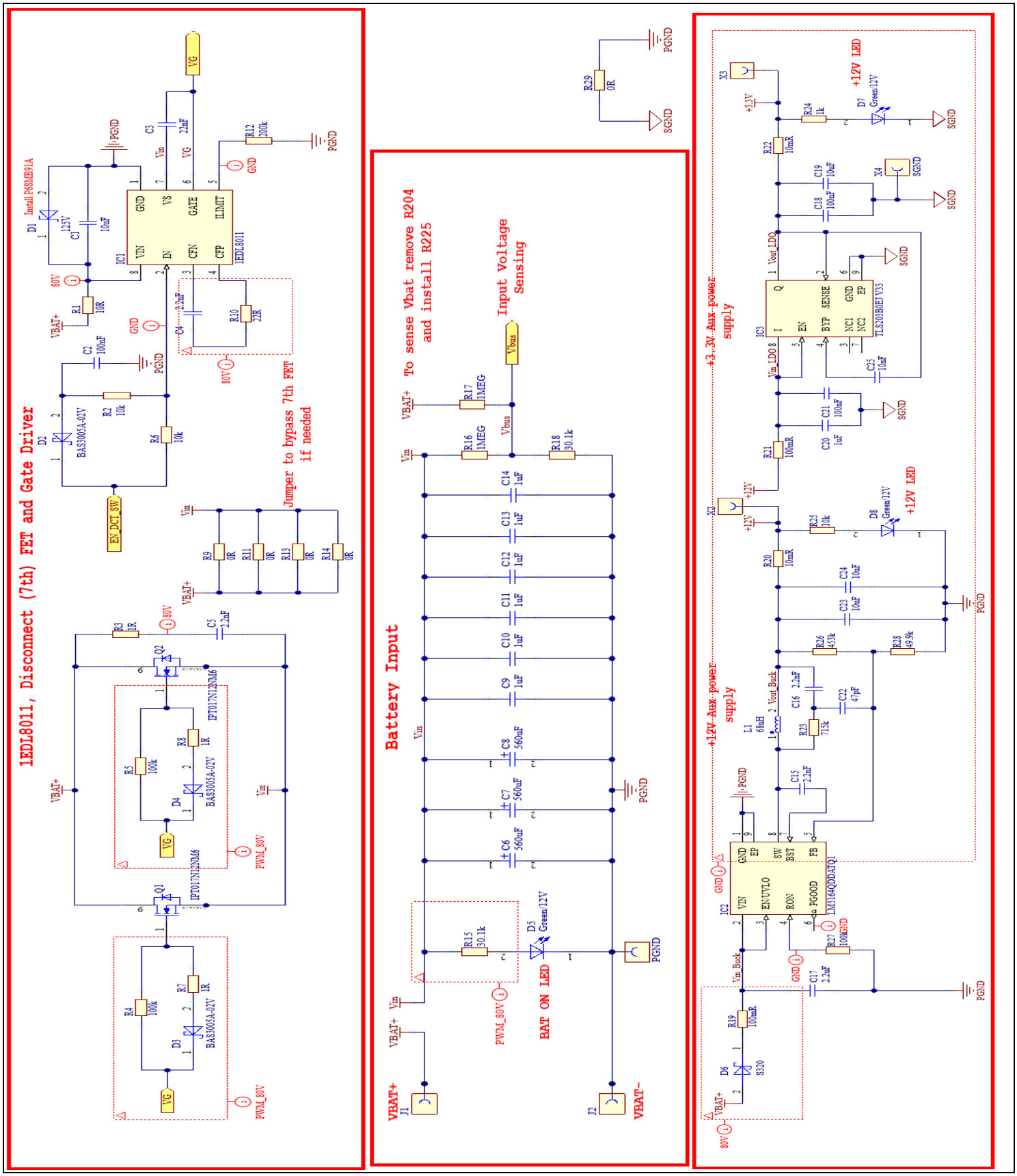

Figure 3 Input stage

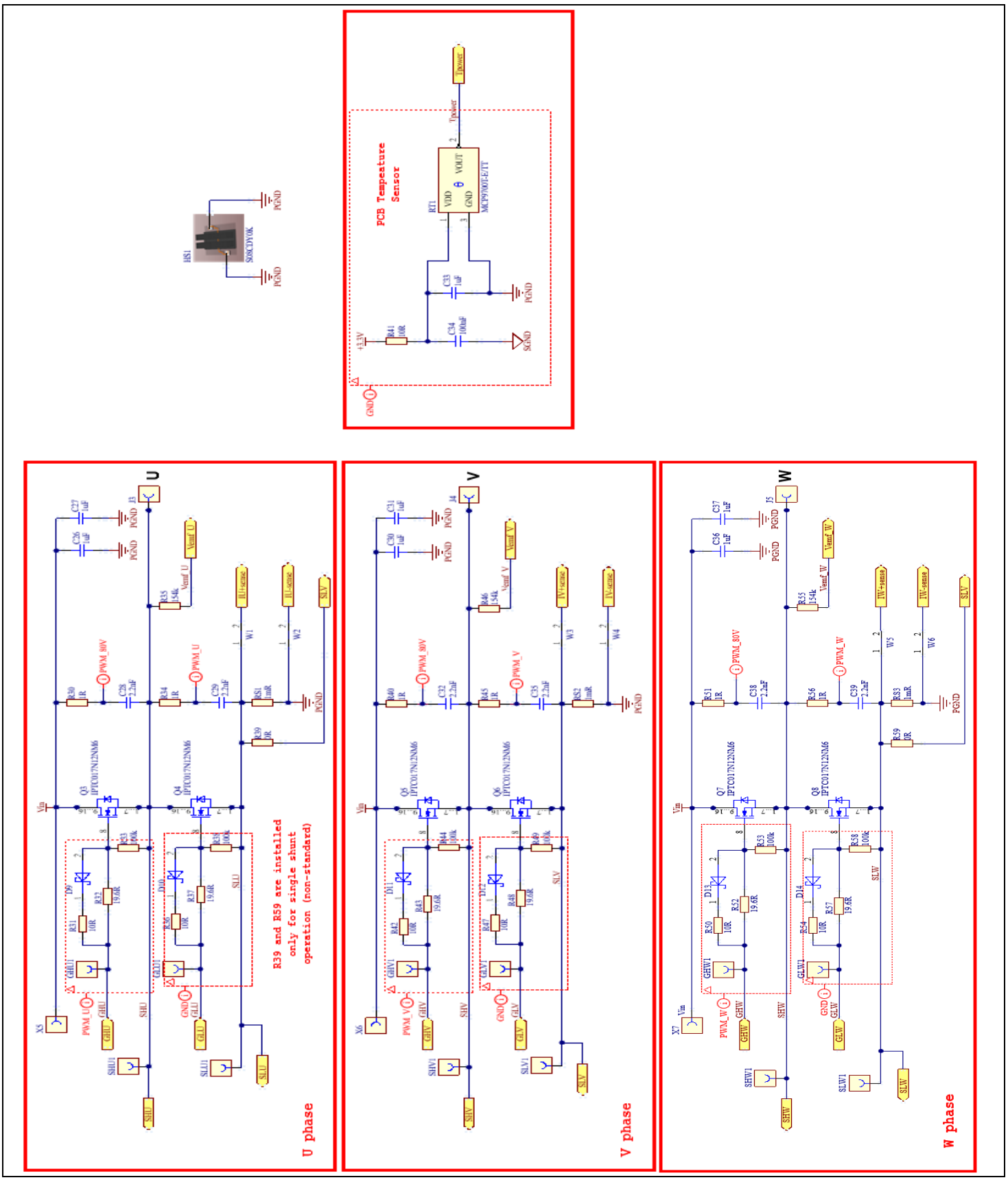

Figure 4 Power stage

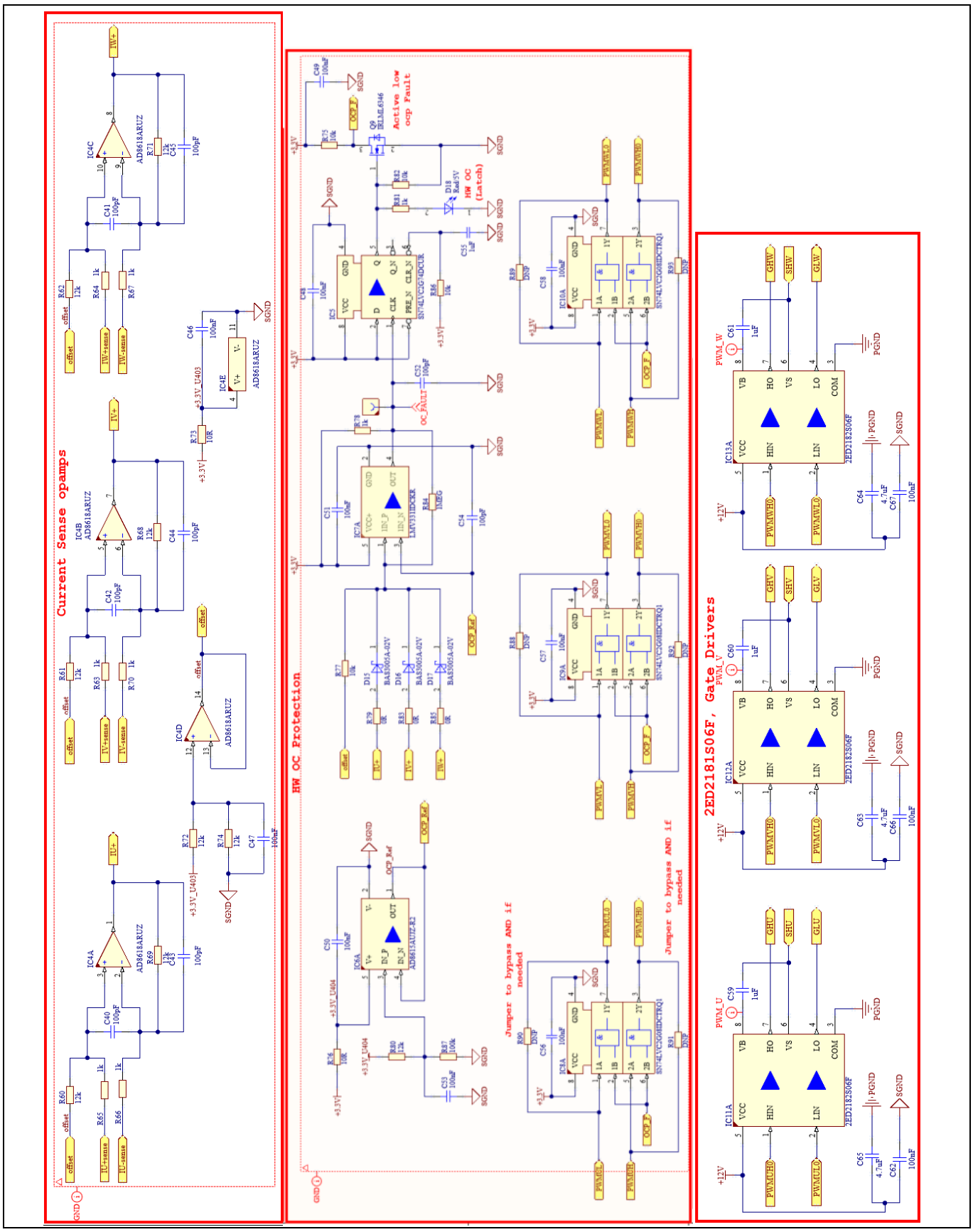

Figure 5 Current sense and driving stage

Schematics

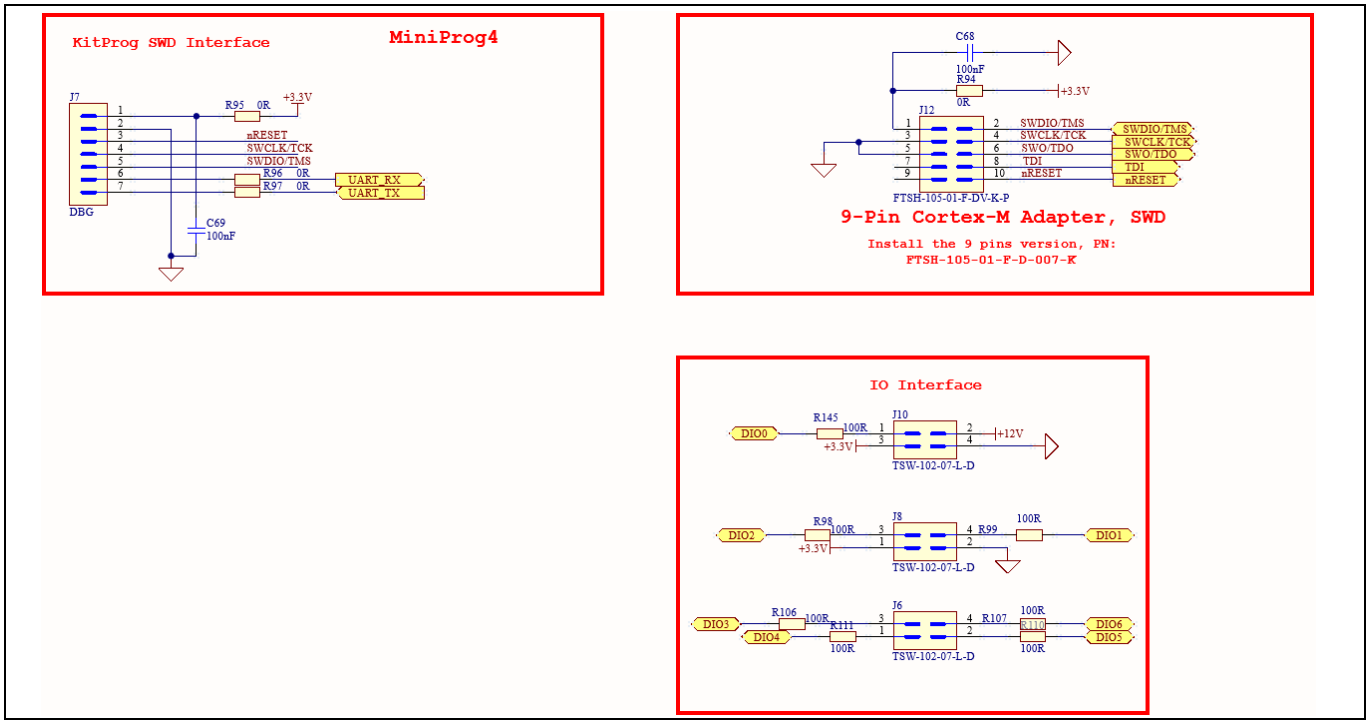

Figure 6 Board connectors

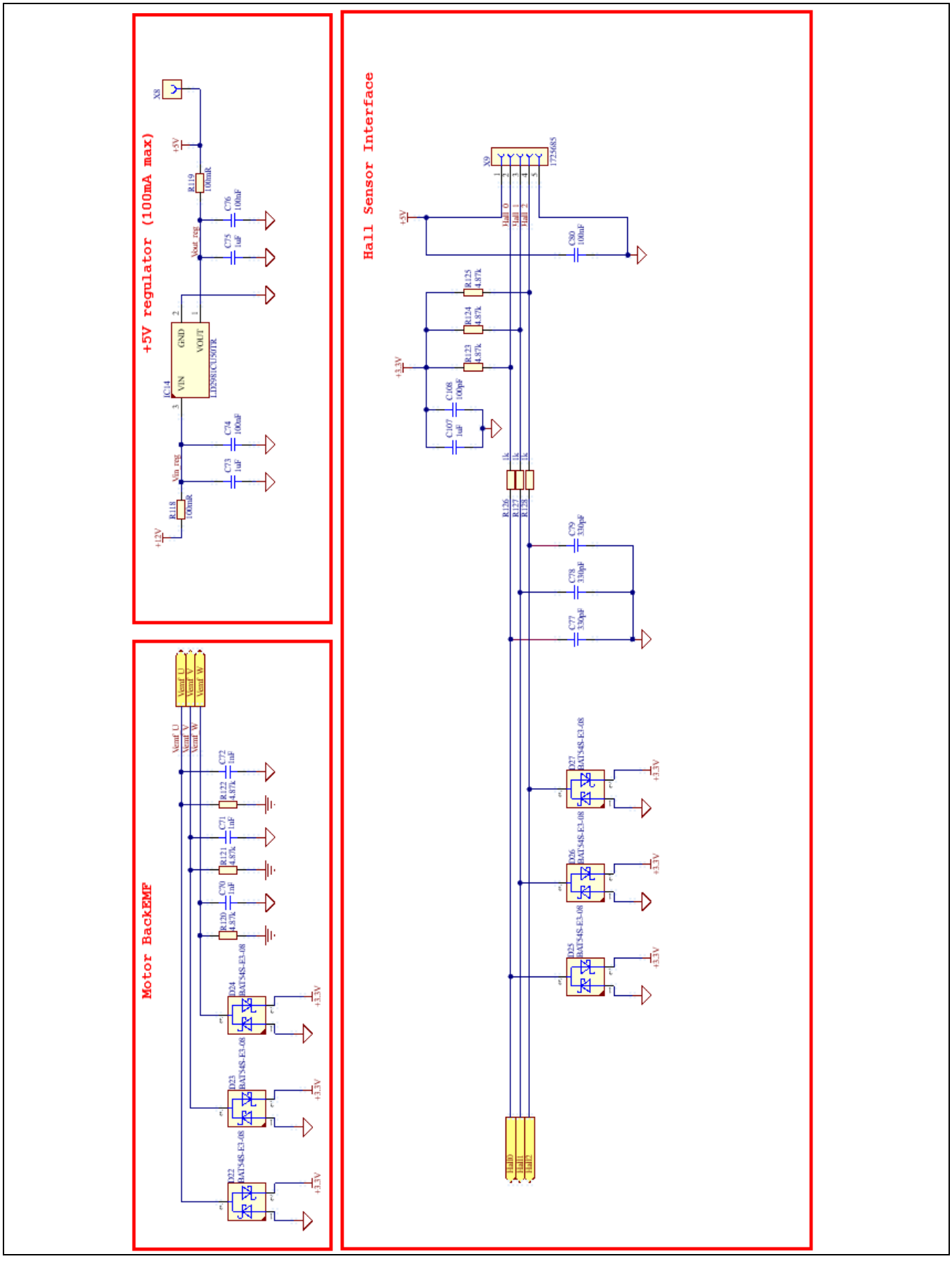

Figure 7 POSIF connectors

Schematics

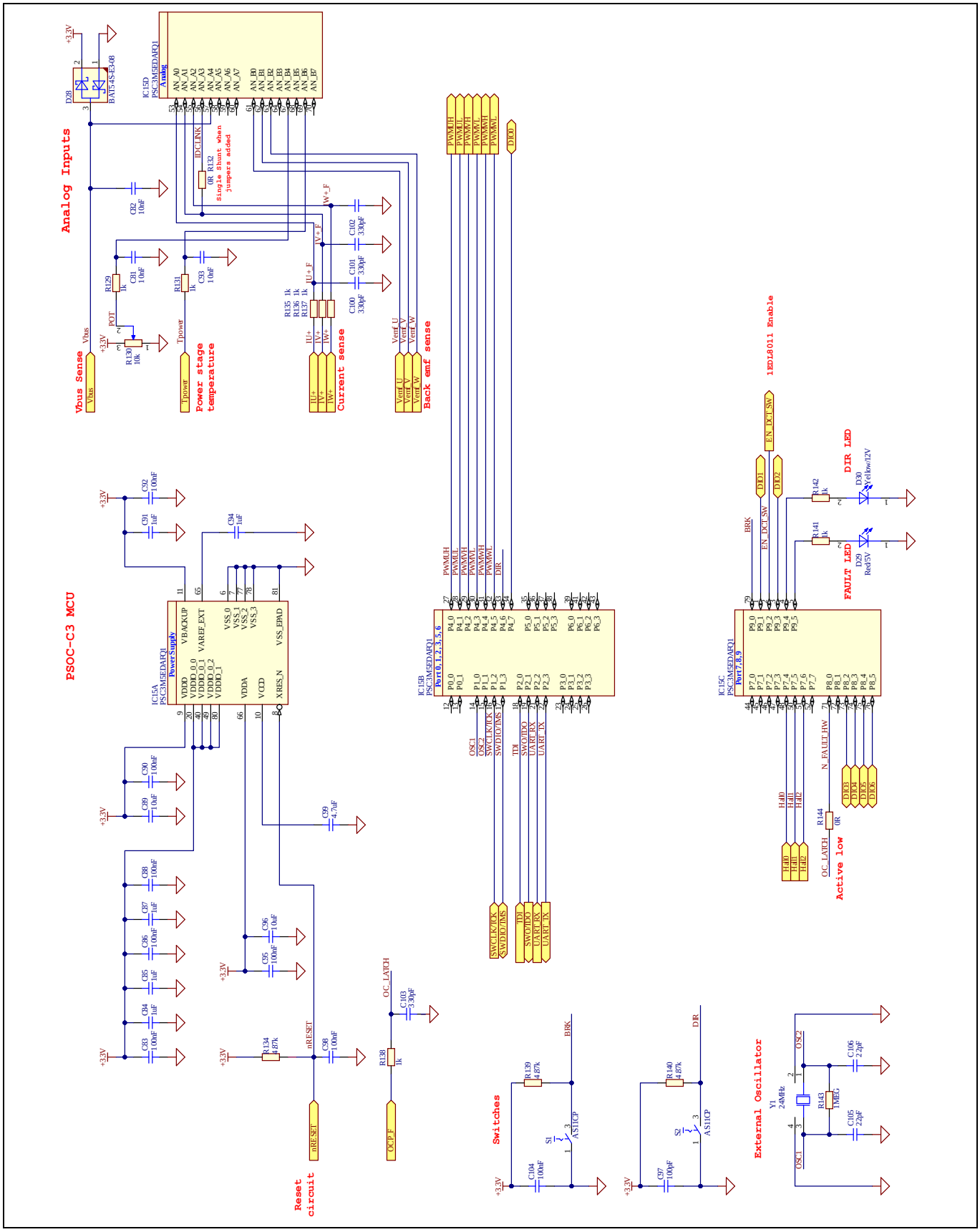

Figure 8 Control stage

4 Hardware functional description

The board is comprised of four stages:

- input stage
- power stage
- current sensing/driving stage
- control stage

As shown in Figure 11, the power stage consists of three half bridges that make up a three-phase inverter. Each half bridge consists of a low-side and high-side MOSFET (IPTC017N12NM6) that are driven by a high- and low-side driver (2ED2181S06F). The driver is supplied by an 80 V voltage through a buck regulator. The output of buck regulator is then stepped down to 3.3 V by a linear voltage regulator that supplies the MCU and other ICs. The ICs on the current sensing and driving circuitry provide protection and sends signals to the MCU in the control stage.

The input stage is a battery disconnect switch consisting of two MOSFETs located at the positive battery input of the board driven by Infineon's EiceDRIVER™ (1EDL8011) gate driver. The driver provides a strong turn on/turn off for a floating gate voltage supply driving the two paralleled MOSFETs using an integrated charge pump. High-side drain-to-source voltage sensing allows the driver to sense a high current fault condition and switch off the MOSFETs to interrupt the battery supply. A series of electrolytic and ceramic capacitors are connected to the source of Q1 and Q2 at the DC bus. The two auxiliary power supplies previously mentioned are located in the input stage and convert the battery voltage to low voltage DC rails. A buck controller (IC2) is used to step down the battery voltage to 12 V while Infineon's TLS203B0 voltage regulator (IC3) is used as the second auxiliary power supply to provide 3.3 V to the microcontroller and other ICs (Figure 9).

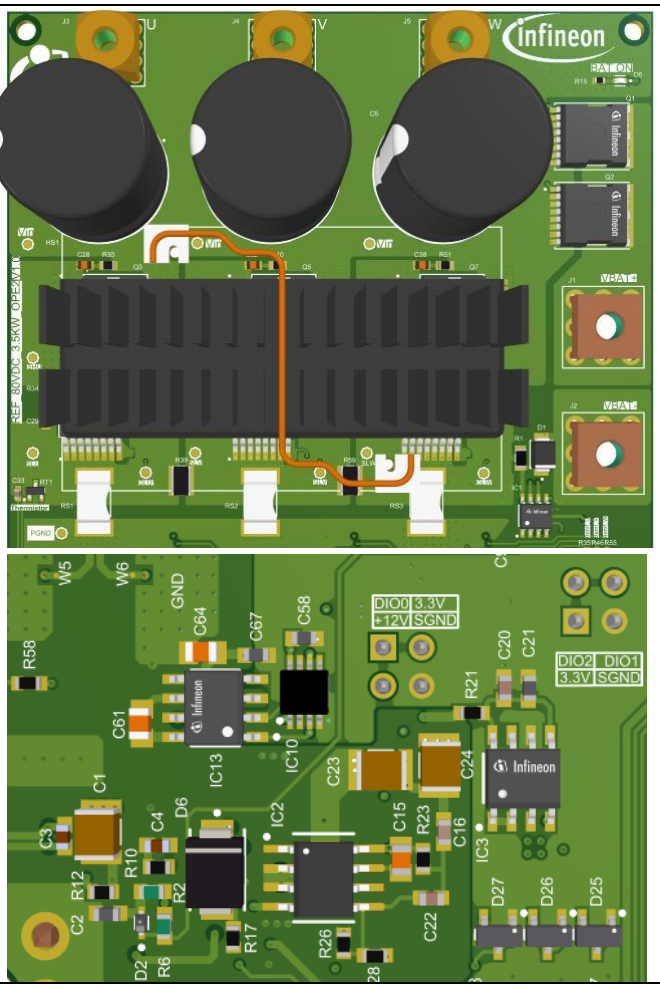

Figure 9 Input stage electrolytic capacitors and MOSFETs

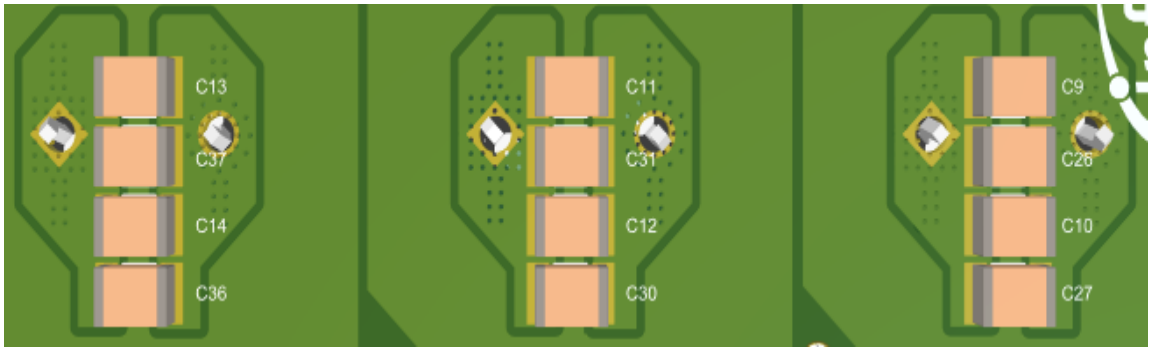

Figure 10 Input stage ceramic capacitors

The power stage has three half bridges that make up a three-phase inverter. Each phase has two TOLT MOSFETs (IPTC017N12NM6) and can support up to 55A_{RMS} phase current for about one minute. The MOSFETs 120 V rating allows headroom for voltage spikes. In addition, a snubber is placed in parallel with each MOSFET to suppress transient drain-to-source voltages. The top-side cooling TOLT MOSFET package allows the heat to dissipate through the heatsink and not the PCB. This maintains a lower junction temperature. For protection purposes, a temperature sensor is placed next to the MOSFETs and the shunts. If the board reaches over 100°C, the system goes into protection mode and shuts down. The reference board is designed to support either single

shunt or three shunt current sensing with three shunts as the default configuration. For normal current sensing operation, three 1 mΩ shunts (RS1, RS2, and RS3) are located on the low-side of each half bridge and ground. For single shunt current sensing, R39 and R59 can be populated with 0 Ω jumpers.

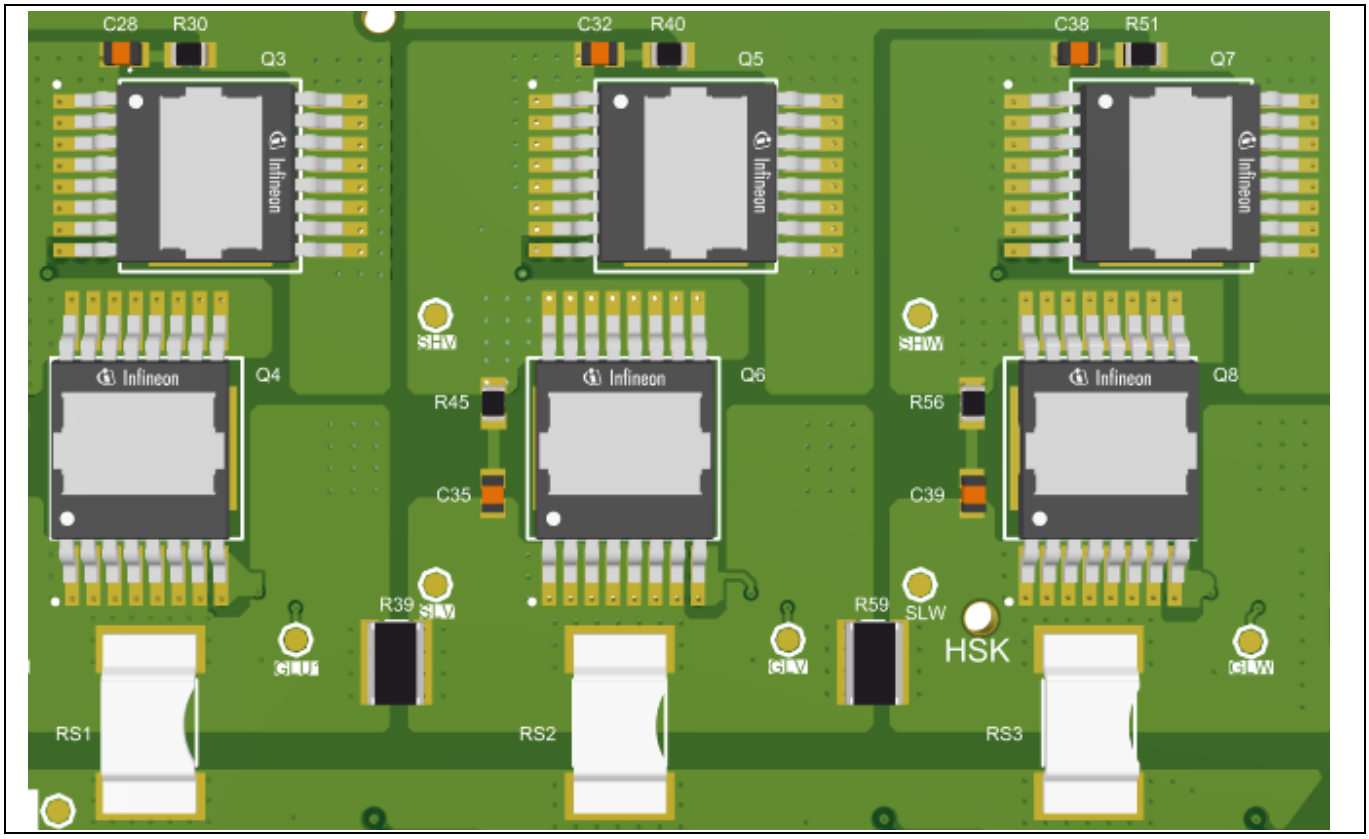

Figure 11 Power stage

As shown in Figure 5, the current sensing/driving circuitry is located directly under the shunts. The voltages produced across the shunts are so small that a voltage-sensing operational amplifier IC (AD8618ARUZ) is necessary to amplify the voltage by a gain of 12. The amplified voltage outputs are then sent to the MCU and the comparator for OCP (overcurrent protection) detection. OCP is crucial in any motor drive design. The comparator (LMV331IDCKR) compares the amplified current signal to the OCP reference. The output of the comparator is then fed to the clock input of the D-flip flop (SN74LVC2G74DCUR). If OCP occurs, the D-flip flop latches and triggers a fault and shuts off the system. If no OCP occurs, the output of the D-flip flop enables the AND gates (IC8, IC9, and IC10) to provide a PWM signal to the gate drivers (IC11, IC12, and IC13).

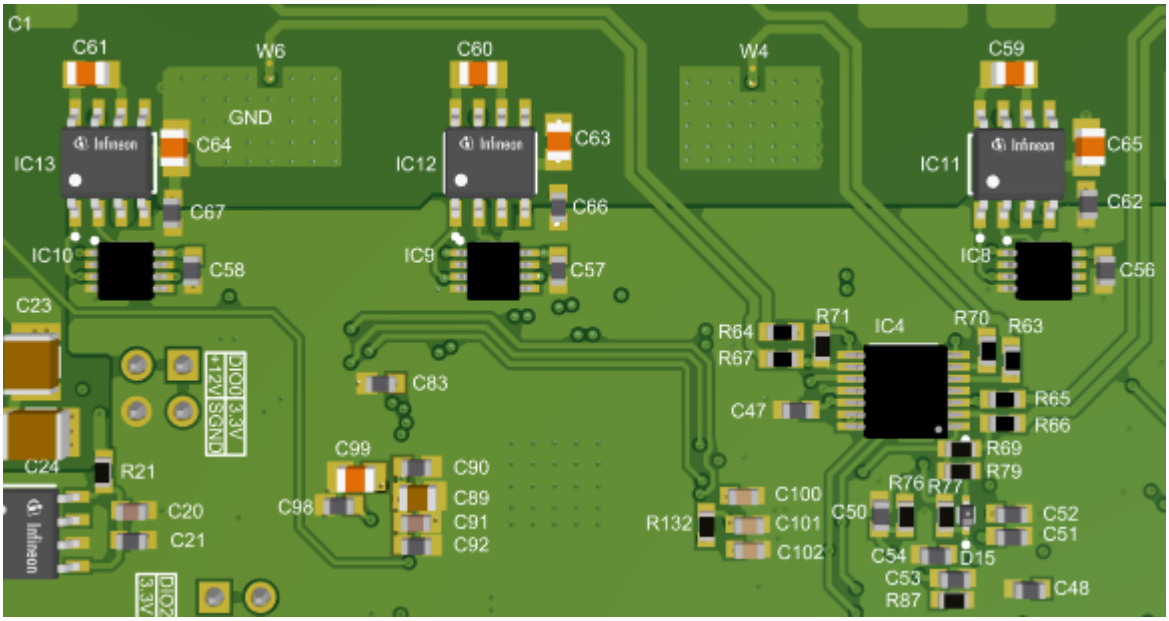

Figure 12 Current sensing/driving circuitry

5 Control and firmware

5.1 Sensorless FOC and trapezoidal control methods

Various control schemes can be used in motor drive applications. The reference board has been designed to support both FOC (Field Oriented Control) and trapezoidal control also known as block commutation. FOC is a control method that allows the rotor to follow the stator maintaining a 90-degree angle between the two flux vectors. The three phase windings are always energized with varying currents in each phase to produce the stator flux angle and magnitude as required. For best performance, three shunts are used to sense the half bridge low side currents, which provide partial phase current feedback sufficient for vector control. Single shunt operation is also possible.

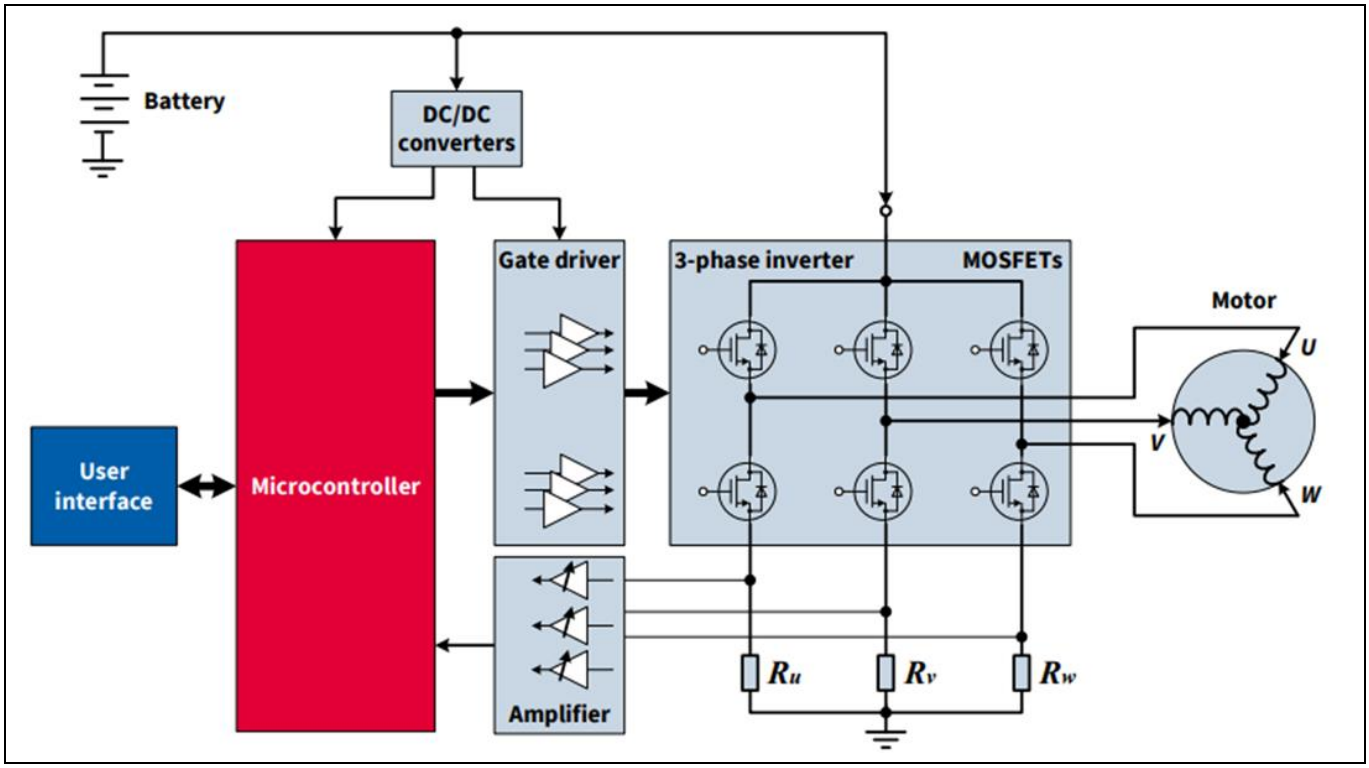

Figure 13 FOC block diagram

These signals are used for sensorless estimation of rotor speed and position. Unlike block commutation in which the angle can vary from 60 to 120 degrees, in FOC the rotor and stator magnetic flux vectors are kept 90 degrees apart to ensure that maximum torque is applied. By achieving maximum torque, the motor will turn optimally and be more efficient due to a low torque ripple, making FOC the preferred control method to use in many applications.

As shown in Figure 12, the three-phase sampled current signals are transformed into two stationary signals using the Clarke transform. The position and rotor speed are then obtained by a sensorless estimator and are used in the Park transform along with the two stationary signals to produce rotating D and Q vectors. Accurate senorless estimation of angle and rotation speed is achieved using calculations in the control firmware and is crucial for keeping the rotor's magnet and the stator field 90 degrees apart.

With FOC, two PI current controllers can be used to control both aspects of the motor current vector separately. One current controller (IQ) is used to control the motor's torque and is thereby called the torque controller while the other one (ID) controls the magnetic flux inside the motor. Transformations are based on the actual rotor angle, which is acquired by position sensors, such as Hall sensors or encoders. The magnetic flux is mainly

generated by the rotor so its target value is usually zero, except in special cases like field weakening where a negative value can be applied to achieve higher speed with lower torque. The magnetic flux is targeted to a value of zero so the PI controller can eliminate direct current and reduce energy loss.

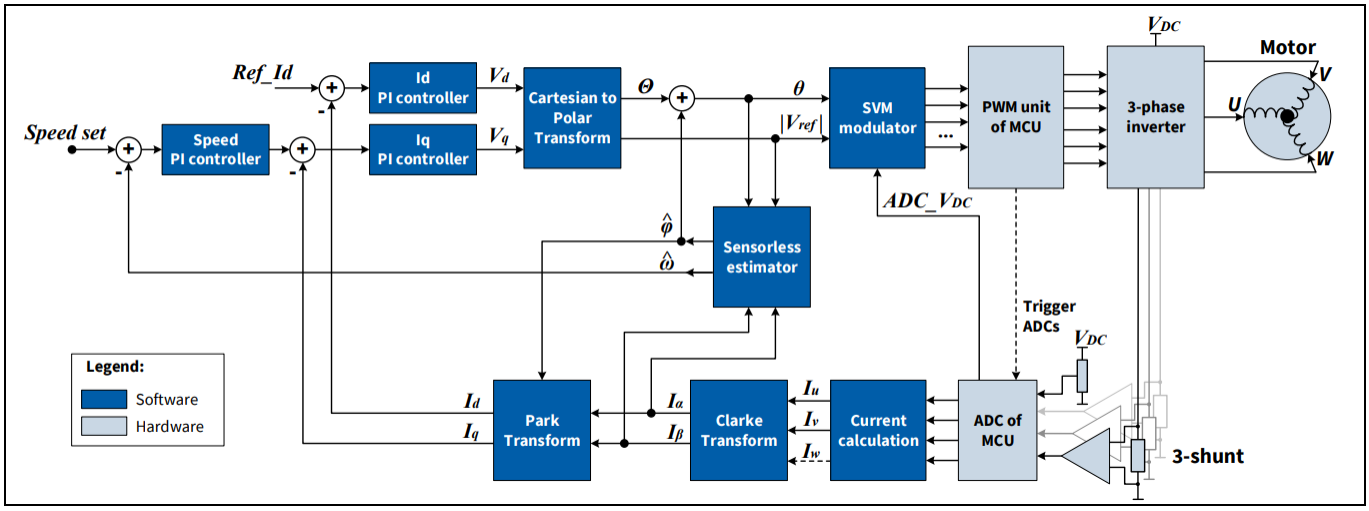

Figure 14 FOC algorithm block diagram

On the other hand, block commutation/trapezoidal control is a simpler control method used in BLDC applications. This control method rotates the motor by energizing two phases for 120 degrees during six phases. As shown in Figure 13, all six phases occur during one electrical period and allow only six stator vector positions. Three MOSFETs are active in each position. During turn-on, the high-side and low-side MOSFETs are active. The low-side MOSFET stays active during turn-on while the high-side turns off and the phase current continues through the body diode of another low-side MOSFET. This causes the angle between the rotor's magnet and stator flux to vary between 60 and 120 degrees as the rotor passes through each sector, which introduces torque ripple. Unlike sensorless FOC, block commutation generally uses Hall or giant magnetoresistance (GMR) sensors to detect the rotor speed and position. The hall sensors then feedback the position to the MCU using hall patterns (Figure 15).

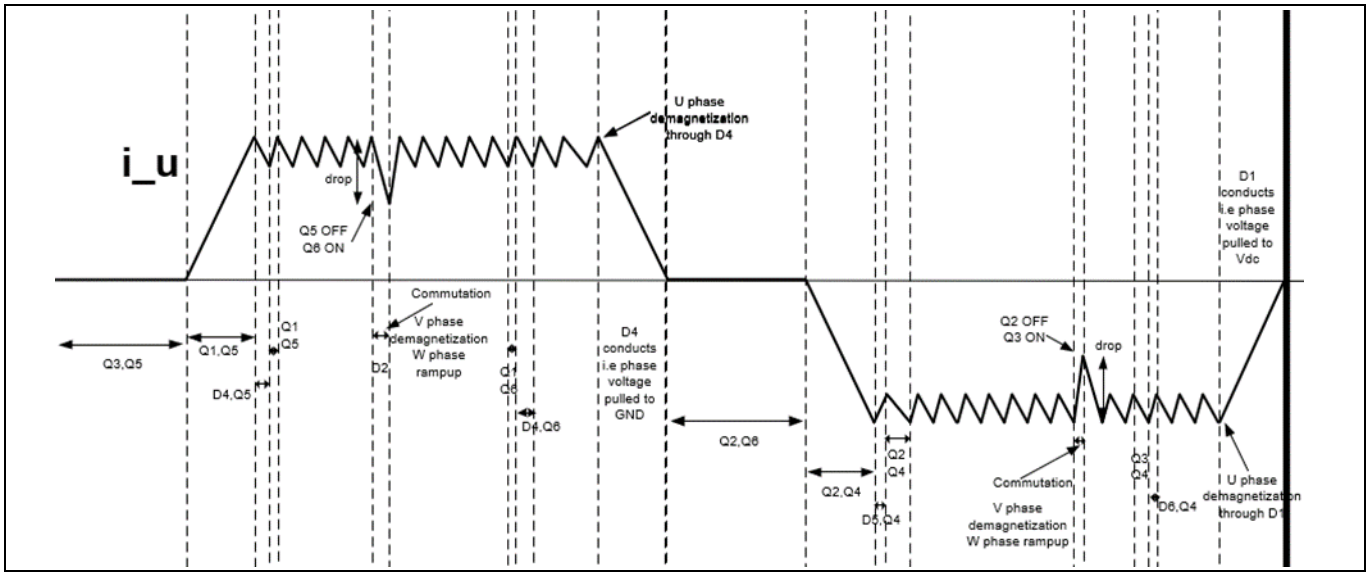

Figure 15 Block commutation electrical period

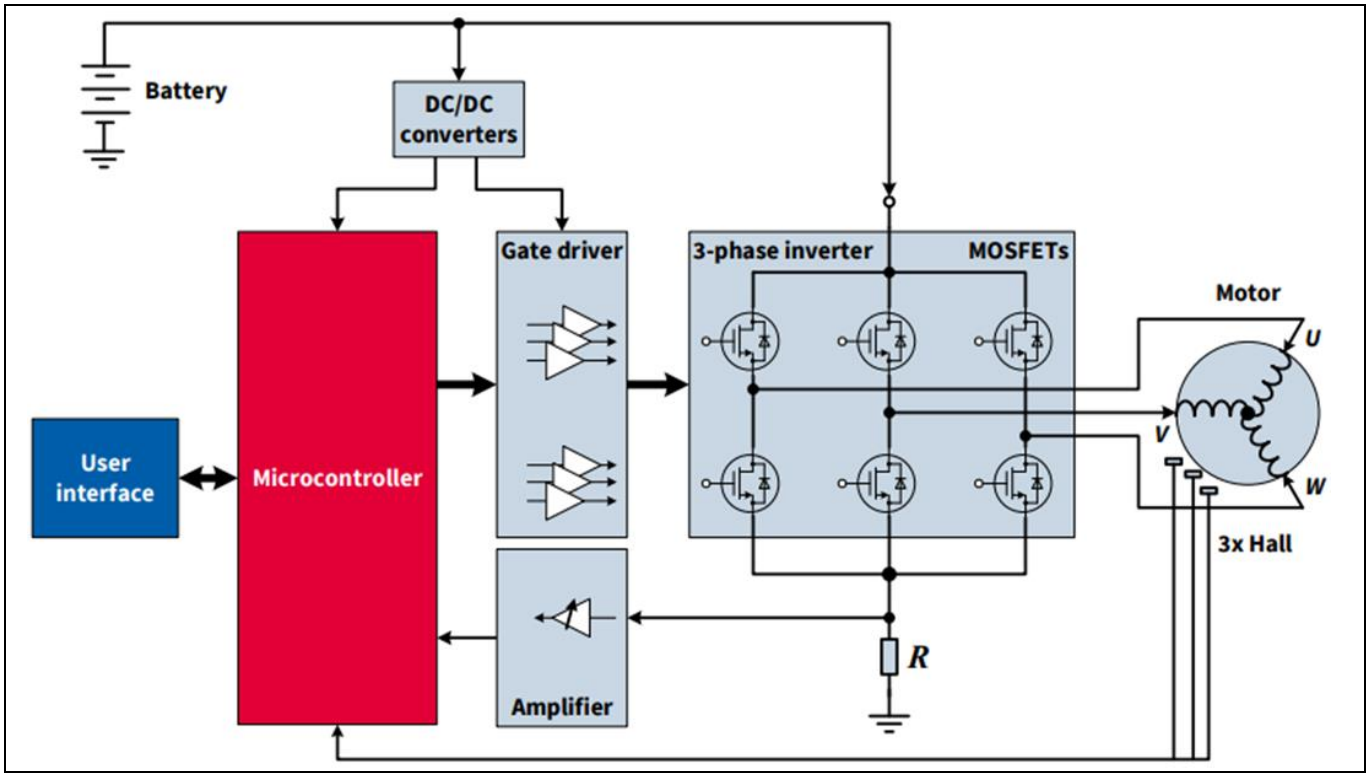

Figure 16 Block commutation block diagram

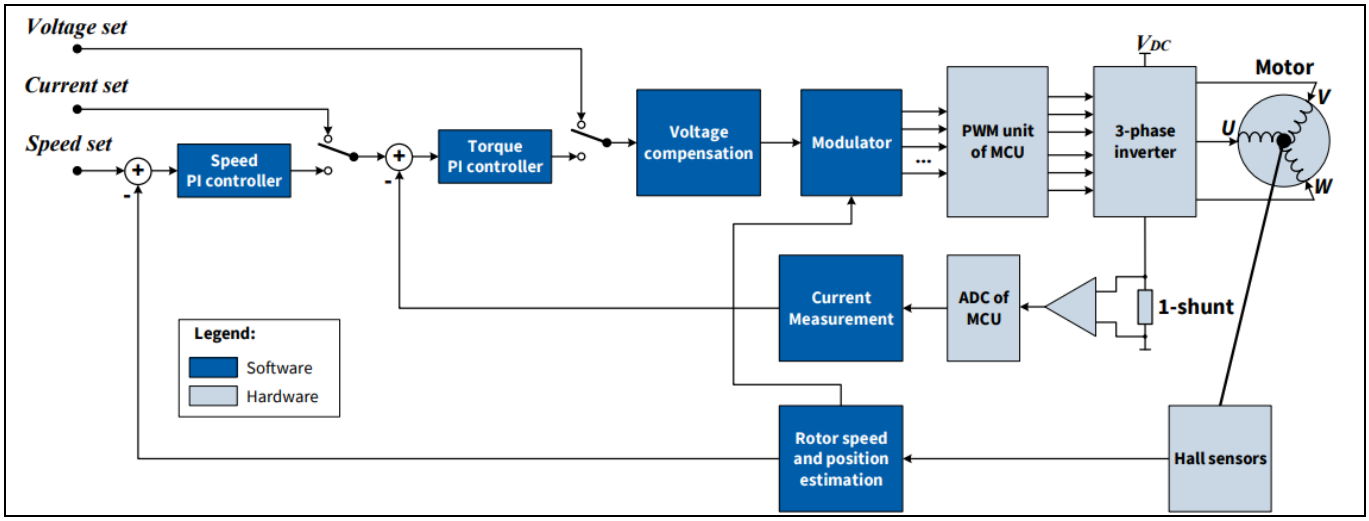

Figure 17 Block commutation algorithm block diagram

FOC and block commutation both differ in hardware and software. As mentioned before, block commutation is a simpler control method. Unlike FOC, block commutation only requires one shunt for current sensing. The Hall sensors are used for sensing the rotor position whereas the position is estimated in FOC by firmware based on the phase currents. The algorithm for FOC is much more complex and requires a complex MCU with greater computing power. The algorithm requires that the signals to go through various mathematical transforms and control loops. Though the results are more efficient, great computing power is needed. Hardware comparison between block commutation and FOC is shown below in Table 1.

Table 1 Hardware comparison of block commutation and FOC

Item	Block Commutation	Sensorless FOC	Comments
Three-phase inverter	Six MOSFETs	Six MOSFETs	Normally N-channel MOSFETs
Gate driver	Three half-bridge gate drivers	Three half-bridge gate drivers	—
MCU	Needs low calculation power	Needs higher calculation power	—
Typical power supply for gate driver	+12 V	+12 V	Other possibilities range from +7 V to 15 V
Typical power supply for MCU	+5 V, from buck converter or LDO	+5 V, preferably from LDO	5 V provides more resolution per ADC least significant bit (LSB). Therefore, 5 V is preferred in FOC.
Current sensing	One leg shunt	Three leg shunts	—
Current sensing amplifiers	One amplifier	Three amplifiers	Three amplifiers enable higher performance in slew rate, bandwidth, and offset error
Rotor Sensor	Three hall sensors	None	FOC uses software to estimate rotor position

5.2 Implementation of field-oriented control

Sensorless FOC based on Infineon's Motor control firmware solution is implemented on the REF_80VDC_3.5kW_OPE2 reference board. The overall block diagram of the SL FOC control method is shown below (Figure 18).

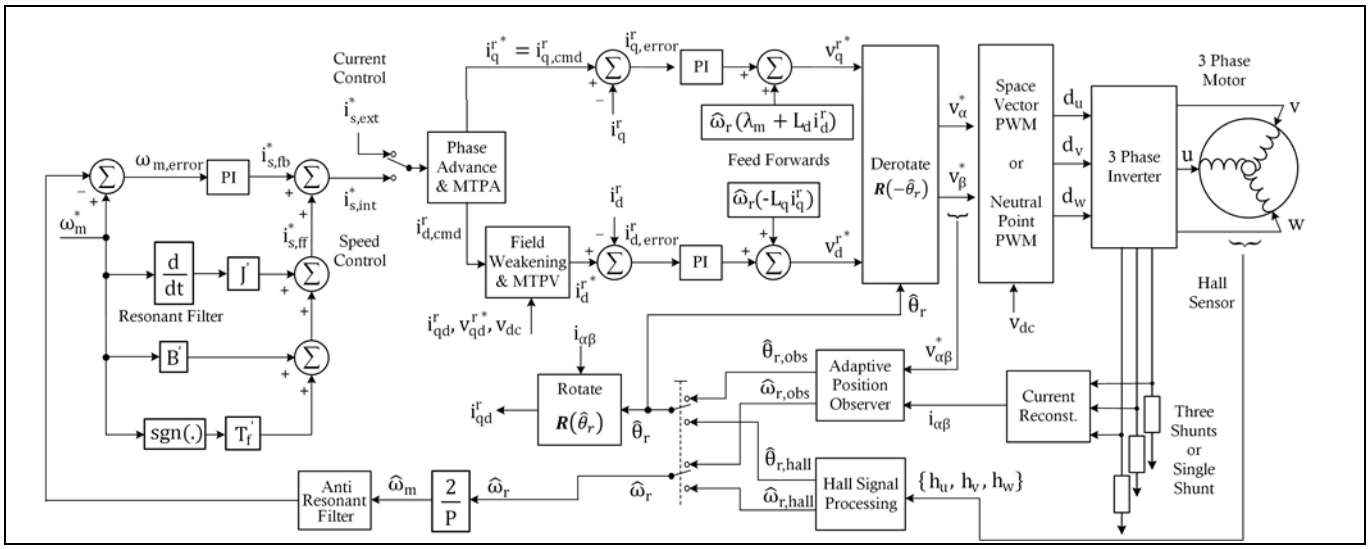

Figure 18 SL FOC block diagram

The position information of the rotor is required to extract the speed and control the q and d axis currents. The position and speed information can be obtained either using a position sensor (such as encoder, resolver, or hall sensors) or through a sensorless approach. The speed controller uses the speed information to create a current reference using a PI controller.

5.3 Speed controller

The parameters of the speed controller are significantly impacted by the mechanical load. The figure below shows the mathematical model of the mechanical load driven by the motor and electrical drive system (Figure 19). This model includes Tf (coulombic friction), B (viscous friction), and J (inertia). When using the firmware to operate any motor, it is crucial to accurately measure or estimate these three parameters and input them into the graphical user interface (GUI) or hard code them in appropriate header files. The speed controller's kp, ki, and feedforward terms are directly derived from these parameters, as explained further.

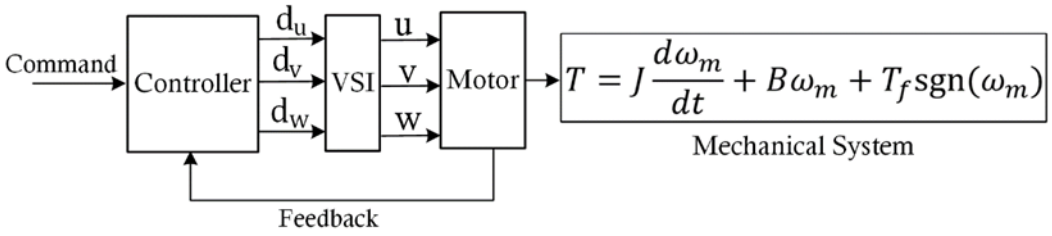

Figure 19 Mechanical load run by motor and drive system

To derive the value of proportional, integral, and feedforward terms of speed controller, the speed loop block diagram along with a simple model of motor and mechanical load will be used, as shown in Figure 20, where:

$$k_t \approx \left(\frac{3}{2}\right)\left(\frac{P}{2}\right)\lambda_m$$

Equation 1

Pole-zero cancellation technique is used to find the PI controller integral and proportional gain. By having

$$\frac{k_i}{k_p} = \frac{B}{J}$$

Equation 2

the controller zero will cancel the mechanical load's pole. The PI controller coefficients are also proportional to speed loop bandwidth, as shown below:

$$k_i \propto B\omega_{BW}$$

Equation 3

$$k_p \propto J\omega_{BW}$$

Equation 4

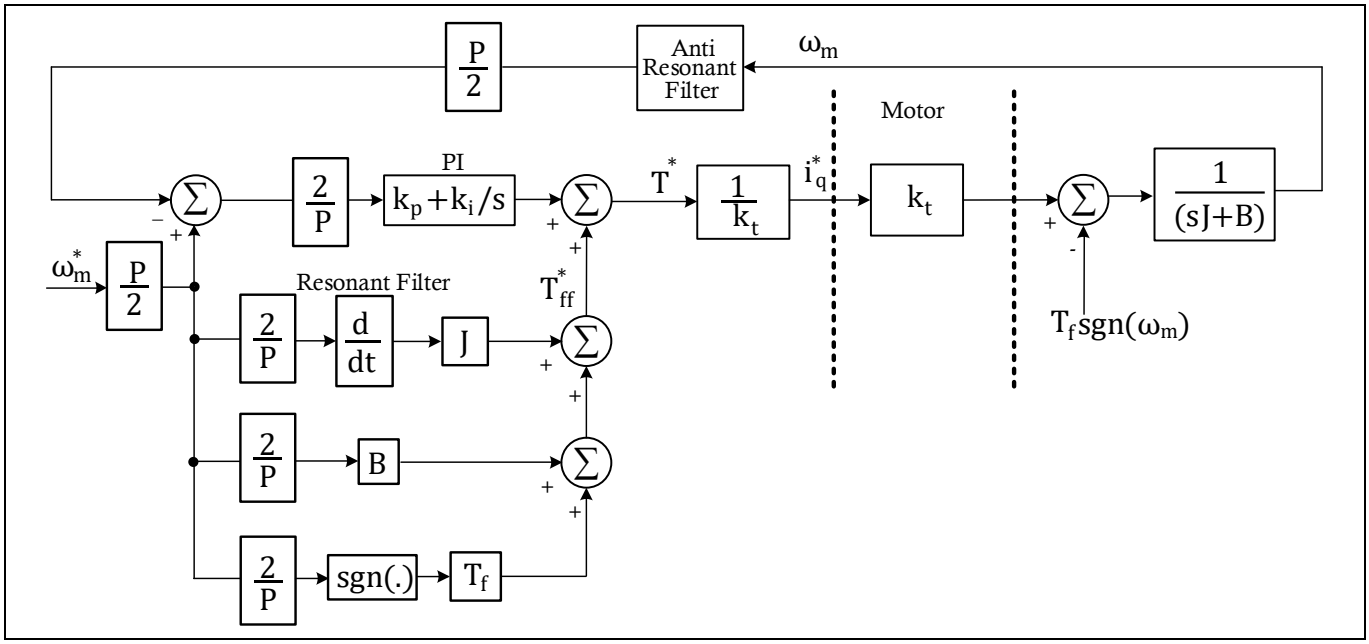

Figure 20 RFO speed control block diagram before rescaling the parameter

The proportional and integral gains are ultimately determined after being rescaled to account for the motor parameters kt and *P*. Figure 21 illustrates how kt and *P*, as shown in Figure 20, can be integrated into the controller parameters, leading to the new updated forms:

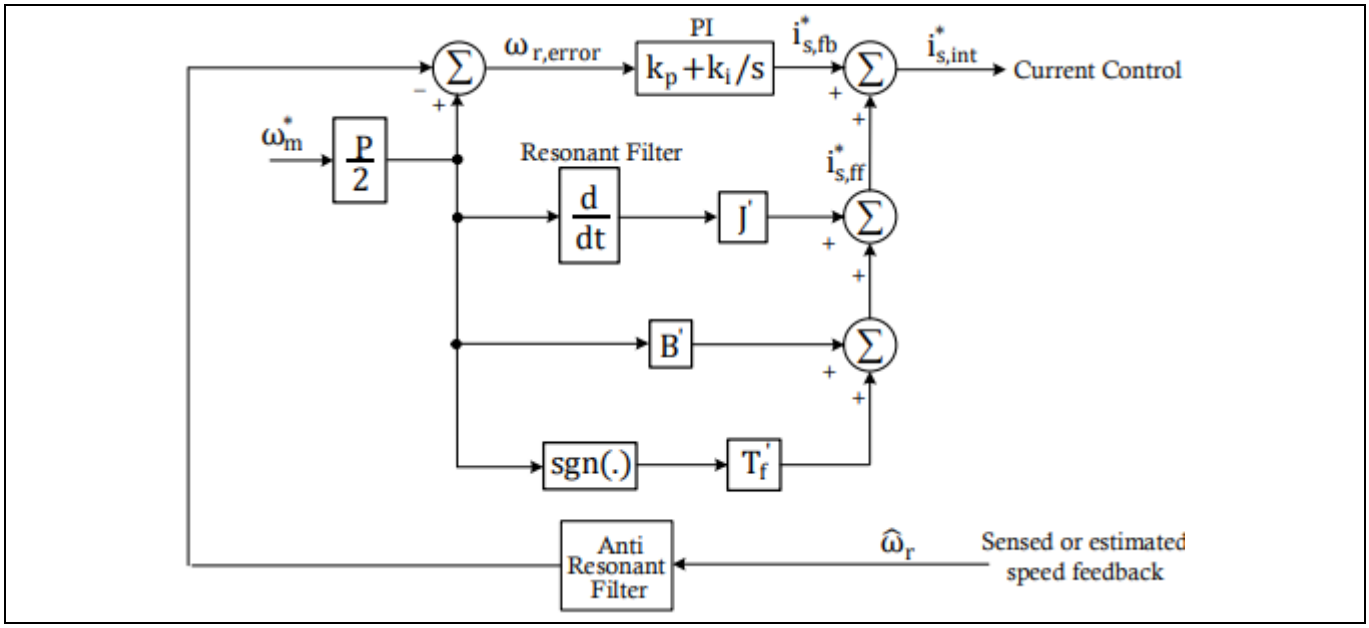

Figure 21 RFO speed loop block diagram before rescaling the parameters

The speed controller parameters after rescaling are:

$$k_i = \left(\frac{1}{k_t}\right)\left(\frac{2}{P}\right) B\omega_{BW} = \left(\frac{8}{3}\right)\left(\frac{1}{P^2}\right)\left(\frac{1}{\lambda_m}\right) B\omega_{BW}$$

Equation 5

$$k_p = \left(\frac{1}{k_t}\right)\left(\frac{2}{P}\right) J\omega_{BW} = \left(\frac{8}{3}\right)\left(\frac{1}{P^2}\right)\left(\frac{1}{\lambda_m}\right) J\omega_{BW}$$

Equation 6

The feedforward terms can also be updated as depicted in the following manner:

$$B' = \left(\frac{1}{k_t}\right)\left(\frac{2}{P}\right) B = \left(\frac{8}{3}\right)\left(\frac{1}{P^2}\right)\left(\frac{1}{\lambda_m}\right) B$$

Equation 7

$$J' = \left(\frac{1}{k_t}\right)\left(\frac{2}{P}\right) J = \left(\frac{8}{3}\right)\left(\frac{1}{P^2}\right)\left(\frac{1}{\lambda_m}\right) J$$

Equation 8

$$T_f' = \left(\frac{1}{k_t}\right) T_f = \left(\frac{4}{3}\right)\left(\frac{1}{P}\right)\left(\frac{1}{\lambda_m}\right) T_f$$

Equation 9

The feedforward terms in the speed loop are affected by both mechanical load and motor parameters. These three feedforward terms play a role in enhancing the dynamic performance of the speed loop. The inertia term utilizes a second-order resonant filter to estimate the acceleration, aiming to mitigate the potential impact of noise that could arise if a direct derivation method was employed.

5.4 Phase advance and MTPA

The MTPA block is responsible for generating command values for q and d axis currents (i_q^r and i_d^r) to maximize the torque for the overall current injected in the motor winding. The torque equation of the PMSM motor is written in Equation 10 as,

$$T = \frac{3P}{4}\left(\lambda_m i_q^r + (L_d - L_q) i_q^r i_d^r\right)$$

Equation 10

The d and q axis current commands $i^{r}_{d,cmd}$ and $i^{r}_{q,cmd}$ need to be obtained from the reference current magnitude i^{*}_{s} generated by the output of the speed controller as follows

$$i^{r}_{d,\mathrm{cmd}} = i^{*}_{s} \sin\theta$$
$$i^{r}_{q,\mathrm{cmd}} = i^{*}_{s} \cos\theta$$

Equation 11

where θ is the angle of the current i^{*}_{s} with respect to rotor q axis

Plugging Equation 11 into Equation 10 and rearranging the whole equation yields the torque equation as a function of θ as,

$$\mathrm{T} = \frac{3P}{4}\left(\lambda_m i^{*}_{s} \cos\theta + \frac{(L_d - L_q)}{2} i^{*2}_{s} \sin 2\theta\right)$$

Equation 12

To find the maximum of the torque function, the equation below needs to be solved

$$\frac{dT}{d\theta} = 0$$

Equation 13

which results in,

$$\sin\theta = \frac{\sqrt{{\lambda_m}^2 + 8(L_d - L_q)^2 i^{*2}_{s}} - \lambda_m}{4(L_d - L_q) i^{*}_{s}}$$

Equation 14

Plugging Equation 14 back into Equation 11 and rearranging, results in MTPA current command values as follows:

$$\mathrm{i}^{r}_{d,\mathrm{MTPA}} = \frac{\lambda_m - \sqrt{{\lambda_m}^2 + 8(L_q - L_d)^2 i^{*2}_{s}}}{4(L_q - L_d)}$$
$$\mathrm{i}^{r}_{q,\mathrm{MTPA}} = \sqrt{i^{*2}_{s} - {\mathrm{i}^{r}_{d,\mathrm{MTPA}}}^2} \cdot \mathrm{sgn}(i^{*}_{s})$$

Equation 15

5.5 Flux weakening and MTPV

Flux weakening (or field weakening) is a method of increasing the motor speed beyond its base speed. At base speed, the inverter voltage becomes saturated, which means that there would not be enough voltage generated on the inverter to overcome the back EMF of the motor and increase the speed above the base speed. Therefore, the flux wakening method is needed to reduce the back EMF voltage of the motor and further increase the speed; Figure 22 illustrates the flux weakening controller for RFO. START HERE EDIT > REVIEW.

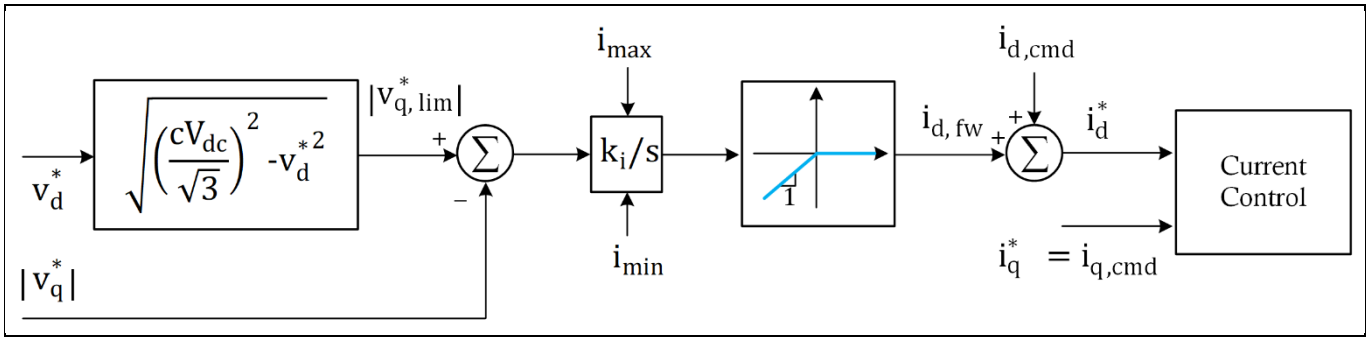

Figure 22 Flux weakening method

As mentioned, the controller requires more voltage, V_q^* than can be produced by the inverter $V_{q,\mathrm{lim}}^*$ above the base limit. Note that the coefficient $c = 0.90 \sim 0.95$ used for the voltage limit is needed to leave some margin before the absolute voltage limitation is reached to avoid instability. The voltage error required to increase the motor speed is passed through an integrator to generate the amount of current in the d axis to weaken the flux and enable speed increase. Note that the current generated by the integrator needs to be limited as follows:

$$i_{\mathrm{max}} = \min\left(KI_{d,\mathrm{max}}, \sqrt{I_{\mathrm{lim}}^2 - i_{q,\mathrm{fb}}^2}\right) - i_{d,\mathrm{cmd}}$$
$$i_{\mathrm{min}} = \max\left(-I_{d,\mathrm{max}}, -\sqrt{I_{\mathrm{lim}}^2 - i_{q,\mathrm{fb}}^2}\right) - i_{d,\mathrm{cmd}}$$

Equation 16

Where $\mathrm{K} = 0.05$ is a coefficient to increase the d axis current saturation level more than zero, $\mathrm{I_{d,max}}$ is the maximum allowable d axis current in the motor and I_{lim} is the maximum three phase allowable current in the motor windings which is determined by the $\mathrm{I^2T}$ protection algorithm. The field weakening current must always be a negative current and be added to MTPA current command $\mathrm{i_{d,cmd}^r}$.

In Equation 16, $I_{d,\mathrm{max}}$ needs to be selected based on the maximum allowable current of the motor and at the same time it must not exceed the level where demagnetization would occur in the rotor magnets. I_{lim} is also the output of $\mathrm{I^2T}$.

5.6 Current controller

The d and q current commands are used as an input for the current controllers and the output would be the voltage references. The voltage references v_d^{r*} and v_q^{r*} are eventually applied to the motor using the inverter to control the current. This means that the voltages are considered as an input to the model of the PMSM machine as:

$$v_d^{r*} = R_s i_d^r + L_d \frac{di_d^r}{dt} - \omega_r (L_q i_q^r)$$
$$v_q^{r*} = R_s i_q^r + L_q \frac{di_q^r}{dt} + \omega_r (\lambda_m + L_d i_d^r)$$

Equation 17

In these equations, the d and q axis currents are not decoupled, and one has a dependency on the other. To decouple this dependency and simplify the equations for the control system, feedforward terms can be added to the output of the current controllers according to Figure 18 and reduce the PMSM system to:

$$v_d^{r*} = R_s i_d^r + L_d \frac{di_d^r}{dt}$$
$$v_q^{r*} = R_s i_q^r + L_q \frac{di_q^r}{dt}$$

Equation 18

Now a PI controller can be easily designed for these set of equations with the equivalent control block diagram shown as followed:

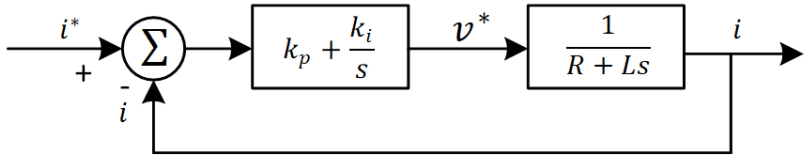

Figure 23 Current controller block diagram

In the closed loop system in Figure 23, it is desired to cancel the pole of the system with the zero of the PI controller to reduce the order of closed loop system and controller design simplification. Hence,

$$\frac{k_p}{k_i} = \frac{L}{R}$$

Equation 19

This will reduce the closed loop transfer function of the system to:

$$H_{cl} = \frac{k_i}{Rs} = \frac{k_p}{Ls}$$

Equation 20

This can be used to calculate the PI controller coefficients for a given system bandwidth ω_c as:

$$k_p = \omega_c L$$
$$k_i = \omega_c R$$

Equation 21

6 Test setup

Various tests were performed on the reference board using the test setup shown in the block diagram below. The oscilloscope along with the voltage and current probes were used to obtain waveforms at various speed and load conditions. The power analyzer was used to measure the efficiency of the reference board at different loads. The board can be controlled using its on-board speed and direction controls or through the ModusToolbox™ Motor Suite software tool (V2.4), which can be downloaded through Infineon Developer installer.

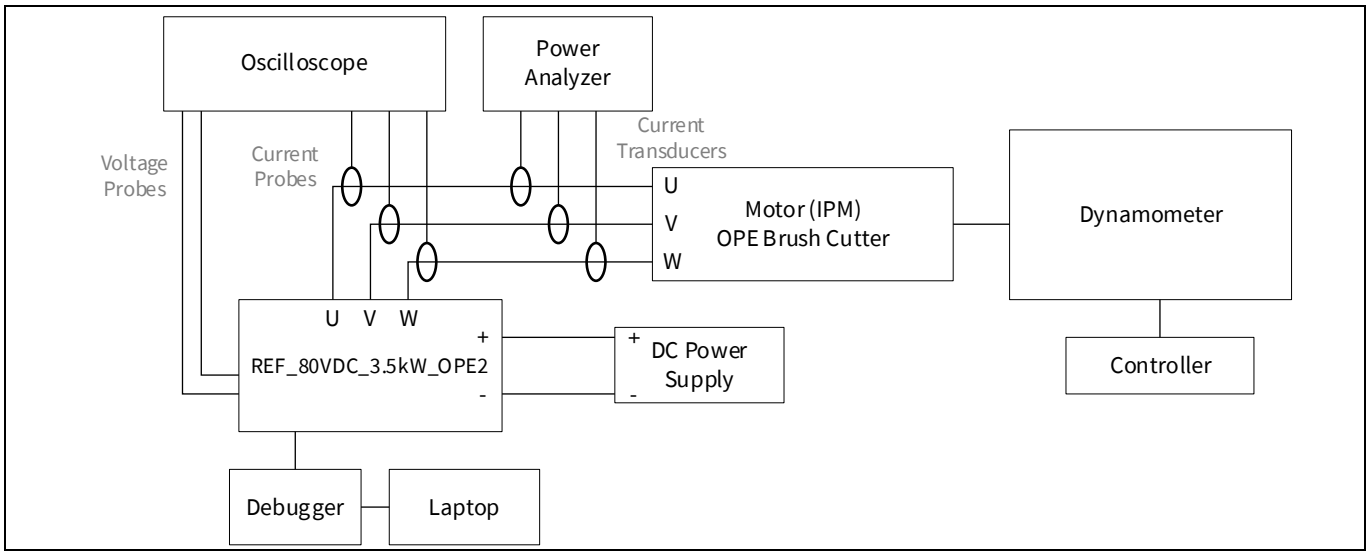

Figure 24 Test setup

The test results were obtained using a Magtrol dynamometer. The dynamometer acts as an adjustable mechanical load that is connected to the test motor and used to measure torque and speed. The reference board was tested under various loads and different speeds, making the dynamometer a practical piece of equipment to use. A blower is connected to the dynamometer and is turned on during testing to prevent the piece of equipment from overheating. In addition, a high-speed programmable controller is connected to the dynamometer and is used to control the torque.

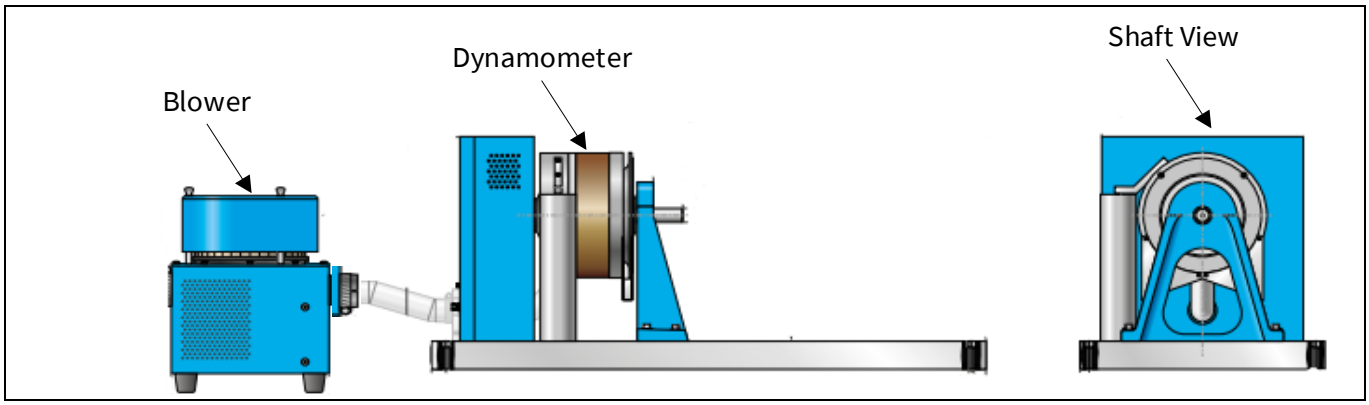

Figure 25 Magtrol dynamometer setup

7 Operating the Board using the motor control GUI

The reference board must be set up properly in order to drive a motor. Figure 26 shows the external connections that are used to connect the motor phases, debugger, power supply, and Hall sensor inputs. Figure 26 also shows the control switches you can use if not using the GUI for controls. Once the external connections are made, the power supply can be set using the proper voltage and current limits and enabled (see specifications). The steps for connecting the board are:

1. Connect the motor cables to the phase terminals on the board (cable order does not matter)
2. Connect the power supply to VBAT+ and VBAT- terminals
3. Set the power supply to 18 V and the current limit to 0.5 A but do not enable the power supply
4. Set the potentiometer to zero (rotate the knob counter-clockwise until it cannot turn anymore)
5. Connect the J-link debugger to the power board
6. Enable power supply. Check that D5, D7, and D6 are lit up

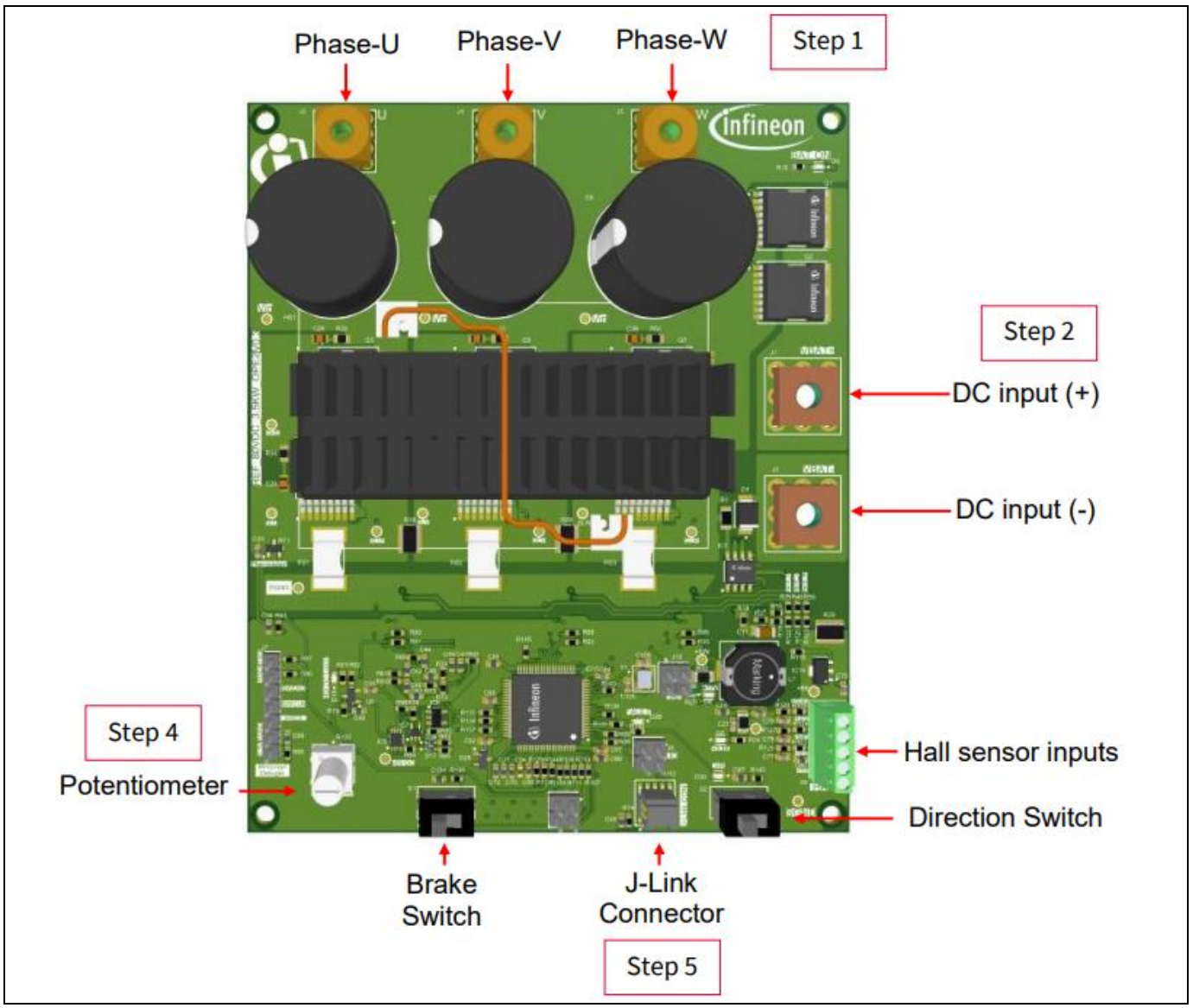

Figure 26 REF_80VDC_3.5KW_OPE2 external connections and controls

Operating the Board using the motor control GUI

The motor control GUI flashes control firmware and configuration settings for the MCU on the motor control boards operating with FOC with one or three shunts. You can use the workbench to select the parameters for a project and then save the configuration. You can also import and flash firmware using the GUI. The steps to downloading and using the GUI are as follows:

1. Download the Infineon Developer Center Launcher application and log in using your Infineon credentials
2. Once the Developer Center Launcher is downloaded, install ModusToolbox™ Motor Suite (V 2.4) by going to **Manage Tools** and searching for it in the search bar

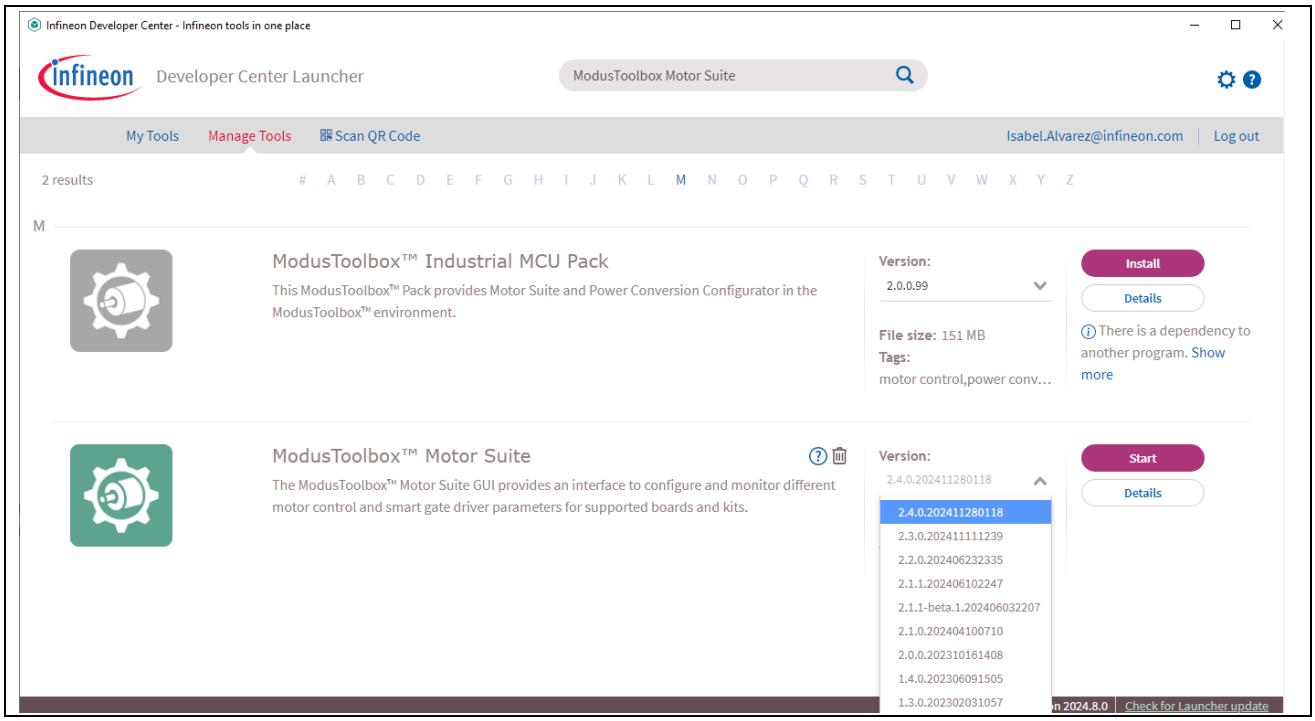

Figure 27 Infineon Developer Center

3. Click **Start** on ModusToolbox™ Motor Suite
4. Create a new project by selecting **PSOC™ Control C3** and selecting **RFO** using the drop-down menu
5. Connect the board to the computer via J-link Debugger and the 80 V power supply
6. Enable power supply and connect the GUI to the board via GUI, as shown on Figure 29
7. Expand the drop-down menu from the **PSOC™-C3** option in the **Parameter Controls** panel

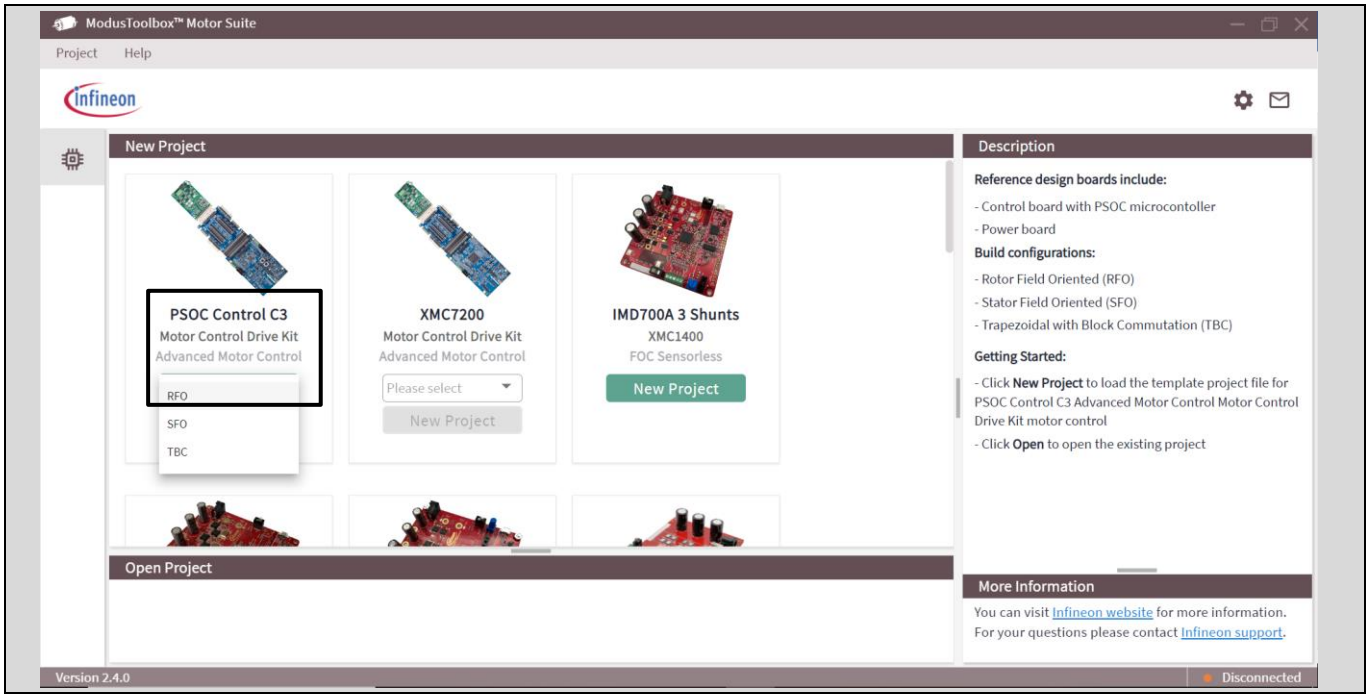

Figure 28 Motor Control GUI launch screen

8. Once the configuration page appears, enable the power supply and connect the GUI to the board by selecting **Disconnected** on the bottom right of the screen and then the **Segger Serial No** option

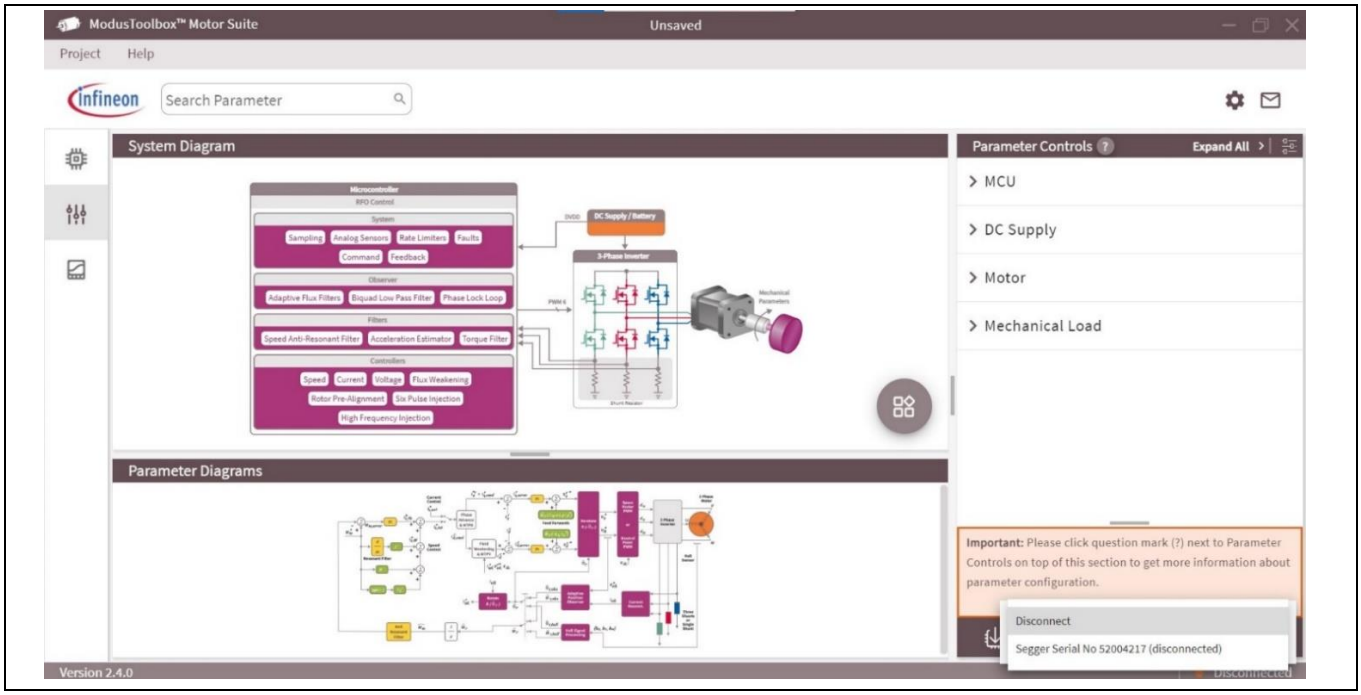

Figure 29 Connecting GUI to Board

9. Edit the motor parameters and voltage supply by opening the drop-down menu for both **DC Supply** and **Motor** on the right-hand side of the screen
10. Flash the parameters by selecting the left bottom symbol shown in Figure 30

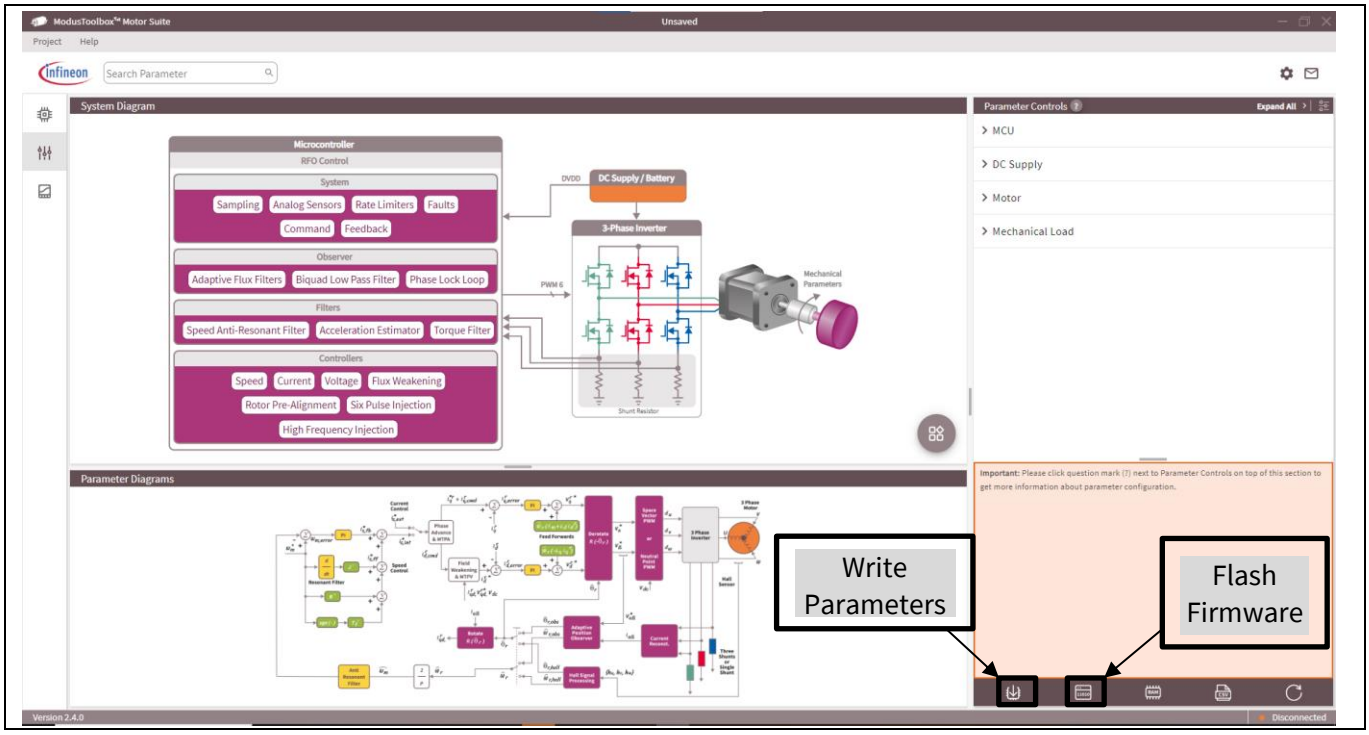

Figure 30 Motor Control GUI configuration page

11. The new values will be highlighted before flashing. Check to see if all the proper parameters were adjusted accordingly and select **Write to Flash**. A message will appear once it has been flashed

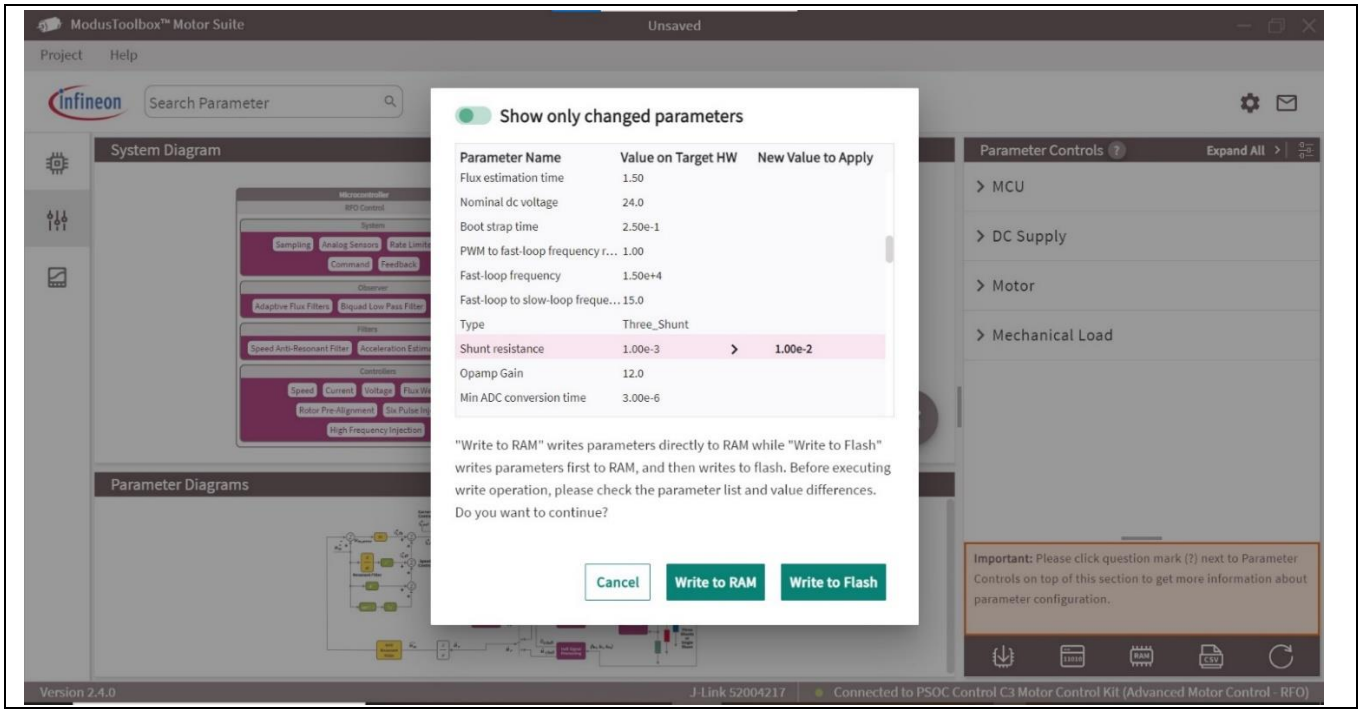

Figure 31 Flashing parameters

12. Go to the Test Bench by selecting the oscilloscope icon on the left-hand side of the screen as shown on Figure 32.
13. On the Command panel, enable **Drive** and start running the board by turning off **Potentiometer Control** and sliding the **Target Set** to the desired speed. If you prefer to run the board using the potentiometer on

the board, turn on the **Potentiometer Control** on the Command panel and increase the speed using the potentiometer on the board

Note: As a precaution, populate R9, R11, R13, and R14 for debugging while using a large load.

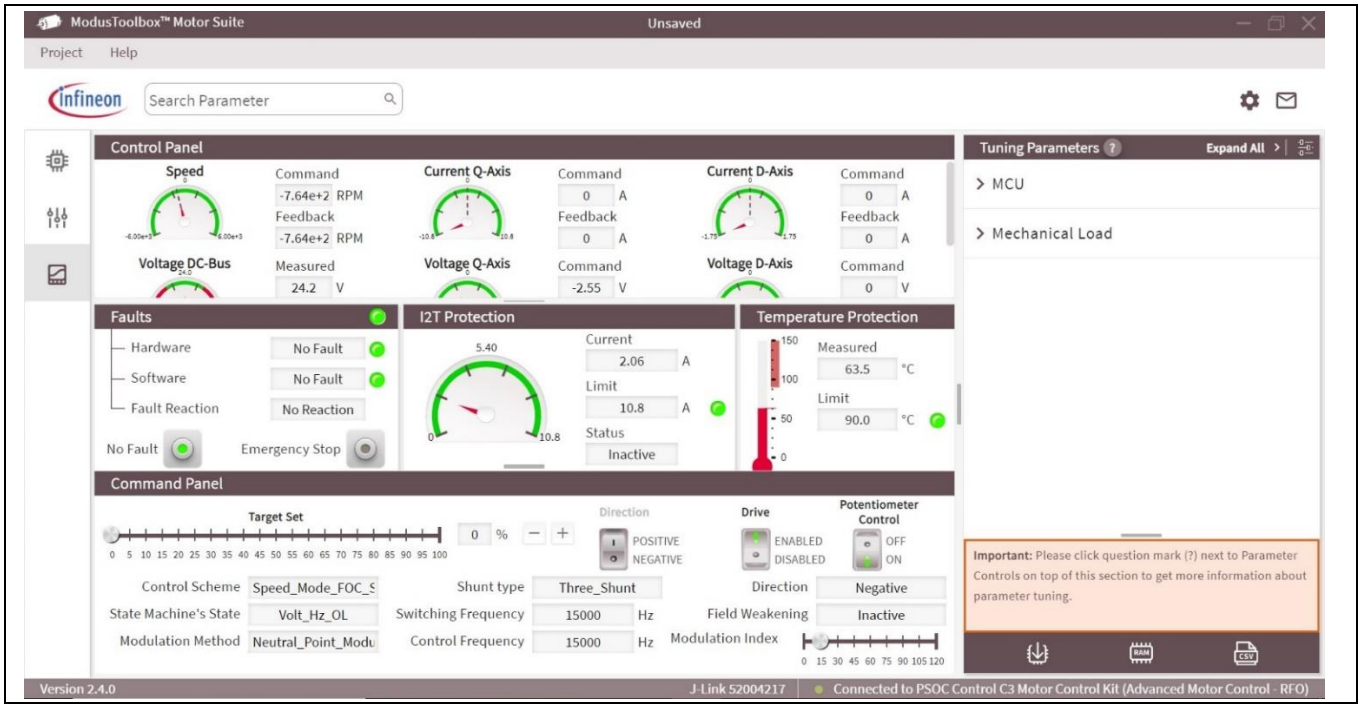

Figure 32 Test Bench

8 Bill of materials

Reference	Qty	Type	Value/rating	Manufacturer	Part number
C1	1	Capacitor	10 uF, 100 V, 10%, 1210, X7S	MuRata	GRM32EC72A106KE05L
C2, C18, C21, C34, C46, C47, C48, C49, C50, C51, C53, C56, C57, C58, C62, C66, C67, C68, C69, C74, C76, C80, C83, C86, C88, C90, C92, C95, C98, C104	30	Capacitor	100 nF, 50 V, 10%, 0603	Kemet	C0603C104K5RACAUTO
C3	1	Capacitor	22 nF, 50 V, 10%, 0603, X8R	TDK Corporation	C1608X8R1H223K080AE
C4	1	Capacitor	2.2 nF, 100 V, 20%, 0603, X7R	TDK Corporation	CGA3E2X7R1H222K080AA
C5, C28, C29, C32, C35, C38, C39	7	Capacitor	2.2 nF, 200 V, 10%, 0805, X7R	Yageo	CC0805KRX7RYBB222
C6, C7, C8	3	Capacitor	560uF, 160 V, 20%, Aluminum electrolytic, THT/Radial	Nichicon	LGG2C561MELZ25
C9, C10, C11, C12, C13, C14, C26, C27, C30, C31, C36, C37	12	Capacitor	1uF, 200 V, 5%, 1812, X7R	Kyocera	18122C105JAT2A
C15	1	Capacitor	2.2 nF, 50 V, 5%, 0805, C0G	TDK Corporation	CGA4C2C0G1H222J060AA
C16	1	Capacitor	2.2 nF, 50 V, 20%, 0603, X7R	TDK Corporation	CGA3E2X7R1H222K080AA
C17	1	Capacitor	2.2uF, 100 V, 10%, 1206, X7R	Samsung	CL31B225KCHSNNE
C19	1	Capacitor	10uF ,25 V, 20%, 0603, X5R	Wurth Elektronik	885012106031
C20, C33, C55, C73, C75, C84, C85, C87, C91, C107	10	Capacitor	1uF, 25 V, 10%, 0603, X7R	Wurth Elektronik	885012206076
C22	1	Capacitor	47 pF, 50 V, 5%, 0603, C0G	TDK Corporation	CGA3E2NP01H470J080AA
C23, C24	2	Capacitor	10uF, 25 V, 10%, 1210, X7R	Samsung	CL32B106KAJNNNE

Bill of materials

Reference	Qty	Type	Value/rating	Manufacturer	Part number
C25	1	Capacitor	10 nF, 25 V, 10%, 0603, X7R	Wurth Elektronik	885012206065
C40, C41, C42, C43, C44, C45, C52, C54, C97, C108	10	Capacitor	100 pF, 50 V, 1%, 0603, C0G	Kemet	C0603C101F5GACAUTO
C59, C60, C61	3	Capacitor	1uF, 50 V, 20%, 0805, X7R	TDK Corporation	CGA4J3X7R1H105M125AE
C63, C64, C65, C99	4	Capacitor	4.7uF, 50 V, 10%, 0805, X7R	TDK Corporation	CGA4J1X7R1H475K125AE
C70, C71, C72	3	Capacitor	1 nF, 50 V, 10%, 0603, X7R	Kemet	C0603C102K5RECAUTO
C77, C78, C79	3	Capacitor	330 pF, 100 V, 2%, 0603, C0G	Cal-Chip Electronics, Inc.	GMC10CG331G100NTD
C81, C82, C93	3	Capacitor	10 nF, 50 V, 10%, 0603, X7R	MuRata	GCM188R71H103KA37J
C89, C96	2	Capacitor	10uF, 10 V, 10%, 0805, X7R	MuRata	GRM21BR71A106KA73K
C94	1	Capacitor	1uF, 16 V, 10%, 0603, X5R	MuRata	GRM185R61C105KE44J
C100, C101, C102, C103	4	Capacitor	330 pF, 50 V, 10%, 0603, X7R	Würth Elektronik	885012206080
C105, C106	2	Capacitor	22 pF, 50 V, 2%, 0603, C0G	Yageo	CC0603GRNPO9BN220
D1	1	Diode	77.8VWM 125VC DO214AA	Bourns Inc.	P6SMB91A
D2, D3, D4, D9, D10, D11, D12, D13, D14, D15, D16, D17	12	Diode	30 V, 500 MA, SC79-2	Infineon Technologies	BAS3005A02VH6327XTSA1
D6	1	Diode	200 V, 3A, DO214AA	ON Semiconductor	S320
D5, D7, D8	3	LED	LED GREEN DIFFUSED 0603 SMD	ams-OSRAM USA INC.	LG Q396-PS-35-0-20-R18
D18, D29	2	LED	LED RED CLEAR 0603 SMD	Dialight	5988010107 F
D30	1	LED	LED YELLOW DIFFUSED 0603 SMD	ams-OSRAM USA INC.	LY Q396-P1Q2-36-0-10-R18
D22, D23, D24, D25, D26, D27, D28	7	Diode	30 V, 200 MA, SOT23	Vishay	BAT54S-E3-08

Bill of materials

Reference	Qty	Type	Value/rating	Manufacturer	Part number
HS1	1	Heat Sink	6063 Aluminum, Black Anodize, 70x25x25, Z-clip	Alpha Co. Ltd	S08CDY0K
IC1	1	IC	Neptune, M1957, A12	Infineon Technologies	1EDL8011
IC2	1	IC	REG, BUCK, ADJ, 1A, 8SOPWR	Texas Instruments	LM5164QDDATQ1
IC3	1	IC	Linear, PG-DSO-8-52	Infineon Technologies	TLS203B0EJ V33
IC4	1	IC	CMOS, 4 CIRCUIT, 14TSSOP	Analog Devices	AD8618ARUZ
IC5	1	IC	FF D-TYPE SNGL, 1BIT, 8VSSOP	Texas Instruments	SN74LVC2G74DCUR
IC6	1	IC	OPAMP, GP 1 CIRCUIT, TSOT23-5	Analog Devices	AD8615AUJZ-R2
IC7	1	IC	COMPARATOR, 1 GEN PUR, SC70-5	Texas Instruments	LMV331IDCKR
IC8, IC9, IC10	3	IC	GATE AND, 2CH, 2-INP, SM8	Texas Instruments	SN74LVC2G08IDCTRQ1
IC11, IC12, IC13	3	IC	IC HALF BRIDGE GATE DRIVER 650 V	Infineon Technologies	2ED2182S06F
IC14	1	IC	REG, LINEAR, 5 V, 100 MA, SOT89-3	STMicroelectronics	LD2981CU50TR
IC15	1	IC	PSOC™, C3, MCU	Infineon Technologies	PSC3M5EDAFQ1
J1, J2	2	Connector	TERM REDCUBE M5 8PIN PCB	Würth Elektronik	74655095R
J3, J4, J5	3	Connector	TERM, REDCUBE, M5, 8PIN, PCB	Würth Elektronik	7460305
J6, J8, J10	3	Connector	CONN HEADER, VERT, 4POS, 2.54MM	Samtec	TSW-102-07-L-D

Bill of materials

Reference	Qty	Type	Value/rating	Manufacturer	Part number
J7	1	Connector	CONN HEADER, VERT, 7POS, 2.54MM	Samtec	TSW-107-07-L-S
J12	1	Connector	CONN HEADER, VERT, 10POS, 1.27MM	Samtec	FTSH-105-01-F-D-007-K
L1	1	Inductor	FIXED IND, 68UH, 1.9A ,132 MOHM, SMD	Würth Elektronik	7447714680
Q1, Q2	2	MOSFET	OptiMOS™ 6, POWER-TRANSISTOR,120 V	Infineon Technologies	IPT017N12NM6
Q3, Q4, Q5, Q6, Q7, Q8	6	MOSFET	N-CH, 120 V, 395 W/331 A, PG-HSOF-8-1	Infineon Technologies	IPTC017N12NM6
Q9	1	MOSFET	N-CH, 30 V, 1.3 W/3.4 A, PG-SOT23-3-901	Infineon Technologies	IRLML6346
R1	1	Resistor	10 R , 0.25 W, 1%, 1206	Vishay	CRCW120610R0FKEA
R2, R6, R25	3	Resistor	10k, 0.1 W, 0.1%, 0603	Vishay	TNPW060310K0BYEA
R3, R30, R34, R40, R45, R51, R56	7	Resistor	1 R, 0.5 W, 1%, 0805	Vishay	CRCW08051R00FKEAHP
R4, R5, R27, R33, R38, R44, R49, R53, R58, R87	10	Resistor	100k, 0.1 W, 1%, 0603	Yageo	RC0603FR-07100KL
R7, R8	2	Resistor	1 R , 0.1 W, 1%, 0603	Yageo	RC0603FR-071RL
R9, R11, R13, R14, R29, R39, R59	7	Resistor	0 OHM, JUMPER, 1 W, 1812	Yageo	RC1218JK-070RL
R10	1	Resistor	22 R, 0.1 W, 1%, 0603	Vishay	CRCW060322R0FKEAC
R12	1	Resistor	200k, 0.1 W, 1%, 0603	Vishay	CRCW0603200KFKEA
R15, R18	2	Resistor	30.1k, 0.1 W, 1%, 0603	Vishay	CRCW060330K1FKEAC
R16, R17, R84, R143	4	Resistor	1MEG, 0.1 W, 1%, 0603	Vishay	CRCW06031M00FKEC

Bill of materials

Reference	Qty	Type	Value/rating	Manufacturer	Part number
R19, R21, R118, R119	4	Resistor	100mR, 0.2 W, 1%, 0603	Yageo	PT0603FR-7W0R1L
R20, R22	2	Resistor	10mR, 1 W, 1%, 1206	Vishay	WSLP1206R0100FEA
R23	1	Resistor	715k, 0.1 W, 1%, 0603	Vishay	CRCW0603715KFKEA
R24, R63, R64, R65, R66, R67, R70, R78, R81, R126, R127, R128, R129, R131, R135, R136, R137, R138, R141, R142	20	Resistor	1k, 0.1 W, 1%, 0603	Panasonic	ERJ3EKF1001V
R26	1	Resistor	453k, 0.1 W, 1%, 0603	Vishay	CRCW0603453KFKEA
R28	1	Resistor	49.9k, 0.1 W, 0.1%, 0603	Panasonic	ERA-3AEB4992V
R31, R36, R42, R47, R50, R54	6	Resistor	10 OHM, 1%, 0.1 W, 0603	Vishay	CRCW060310R0FKEA
R32, R37, R43, R48, R52, R57	6	Resistor	19.6 OHM, 1%, 0.1 W, 0603	Vishay	CRCW060319R6FKEA
R35, R46, R55	3	Resistor	154k, 0.1 W, 1%, 0603	Vishay	CRCW0603154KFKEA
R41, R73, R76	3	Resistor	10 R, 0.1 W, 1%, 0603	Yageo	RC0603FR-0710RL
R60, R61, R62, R68, R69, R71, R72, R74, R80	9	Resistor	12k, 0.1 W, 1%, 0603	Yageo	RC0603FR-0712KL
R75, R77, R82, R86	4	Resistor	10k, 0.1 W, 5%, 0603	Yageo	RC0603JR-0710KL
R79, R83, R85, R88, R89, R90, R91, R92, R93, R94, R95, R96, R97, R132, R144	15	Resistor	0 OHM, JUMPER, 0.1 W, 0603	Yageo	RC0603JR-070RL
R98, R99, R106, R107, R110, R111, R145	7	Resistor	100 R, 0.1 W, 1%, 0603	Panasonic	ERJ-3EKF1000V
R120, R121, R122, R123, R124, R125, R134, R139, R140	9	Resistor	4.87k, 0.1 W, 1%, 0603	Vishay	CRCW06034K87FKEA

Bill of materials

Reference	Qty	Type	Value/rating	Manufacturer	Part number
R130	1	Potentiometer	10k, 0.5 W, 10%, THT	Bourns	3362P-1-103T_LF
RS1, RS2, RS3	3	Resistor	1mR, 8 W, 1%, 0402	Bourns	CSS2H-3920R-1L00F
RT1	1	Sensor	SENSOR ANALOG, -40C-125C, SOT23-3	Microchip Technology	MCP9700T-E/TT
S1, S2	2	Slide Switch	SWITCH SLIDE SPST 0.4 VA 28 V	NKK Switches	AS11CP
X9	1	Terminal Block	TERM BLK 5P SIDE ENT 2.54MM PCB	Phoenix Contact	1725685
Y1	1	Clock	CRYSTAL, 24.000 MHZ, 8 PF, SMD	ECS Inc	ECS-240-8-33B-CWN-TR

9 PCB layout

The REF_80VDC_3.5KW_OPE2 reference board utilizes a six-layer PCB with 2 oz. copper for each layer. The multiple layers help dissipate heat when the board is running at high power. Components are mounted on the top and bottom sides. The dimensions are 4.05 inches/102.98 mm x 4.92 inches/125 mm.

The top and the middle third layers are designated power planes. The battery voltage, voltage input (V_{in}), and power ground are routed through the two layers via terminals (BATT+, PGND, and V_{in}). Both layers each have four nets and share three of those nets. The bottom polygon on each layer contains different nets. The bottom polygon on the top layer is designated for routing analog ground and the bottom polygon of the third middle layer used to route 3.3 V. The ICs that require 3.3 V are placed on the bottom polygon. The top layer is used for carrying high current and routing components that require a higher input voltage, such as the electrolytic capacitors, shunts, and MOFETs. Other signal layers are purposely placed in between the power layers to allow effective heat dissipation. As shown in Figure 33, electrolytic capacitors are placed close to the battery terminals to filter out unwanted noise and high ripple. The MOSFETs are also placed close to the battery terminals to minimize the parasitic inductance. This helps reduce voltage drops and creates a smaller loop area for the current path.

The first and fourth middle layers are designated ground planes that are shorted out via R29. The top portion of both layers is designated for power ground and the bottom portion below the shunts is designated for analog ground. The fourth middle layer is not only utilized for ground nets but also contains Vin polygons. The components carrying high current are placed on the top half of the board to minimize EMI interference and provide a low-impedance return path of currents. As mentioned earlier, the bottom portions of both layers are reserved for analog signals and grounding. ICs that require low current are placed in the bottom portion to minimize high impedance and parasitic.

The second middle layer and bottom are used for phase connections. Both layers contain large polygons that support high current to flow through the phases, shunts, and MOSFETs. A large polygon runs from the top of the phase terminals to the high-side of the three-phase inverter while another polygon runs from the low-side of the inverter to the shunts. Both layers support the same nets, however, the second middle layer contains a polygon with a 12 V net used to route ICs that require 12 V.

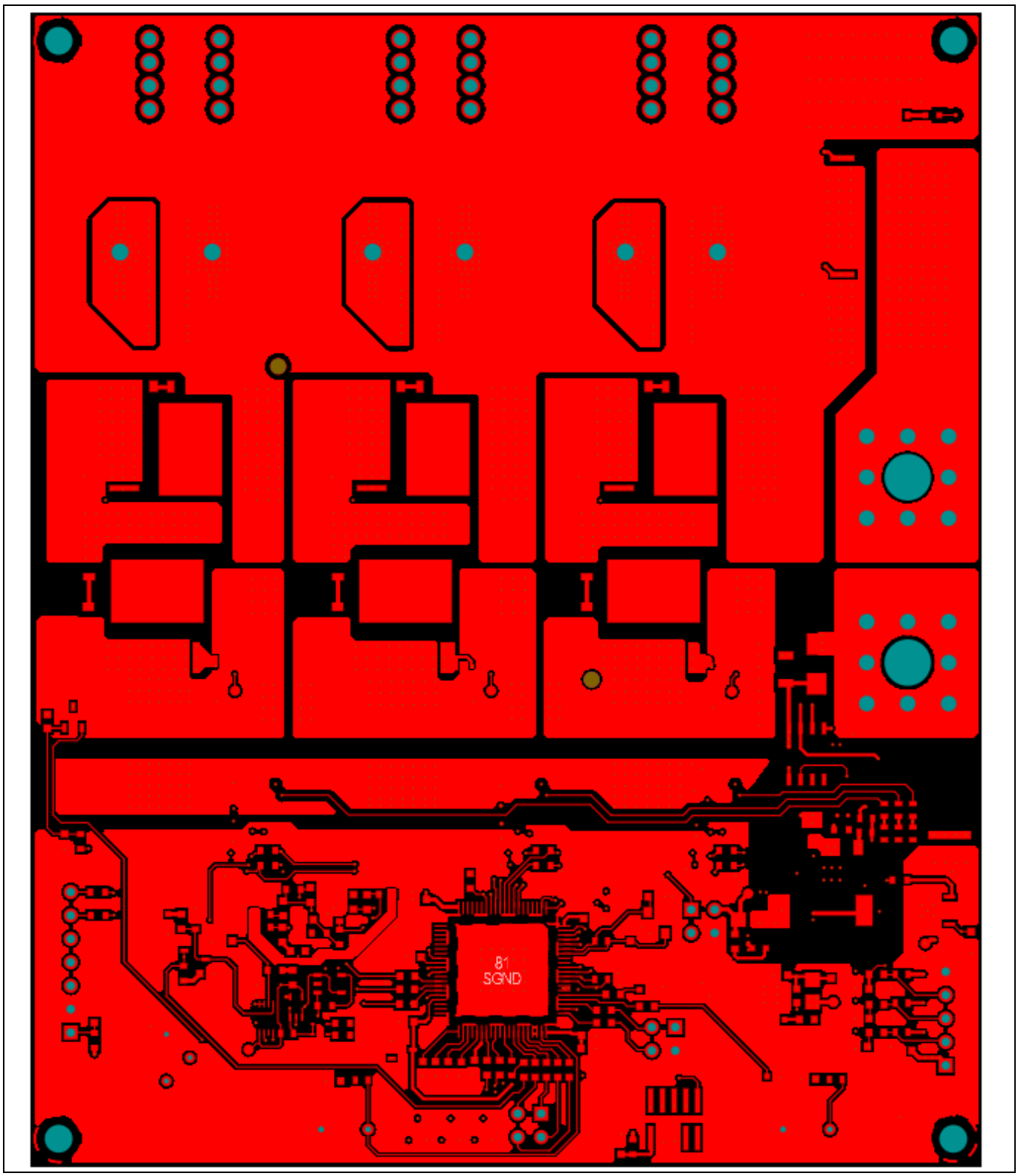

Figure 33 Top layer

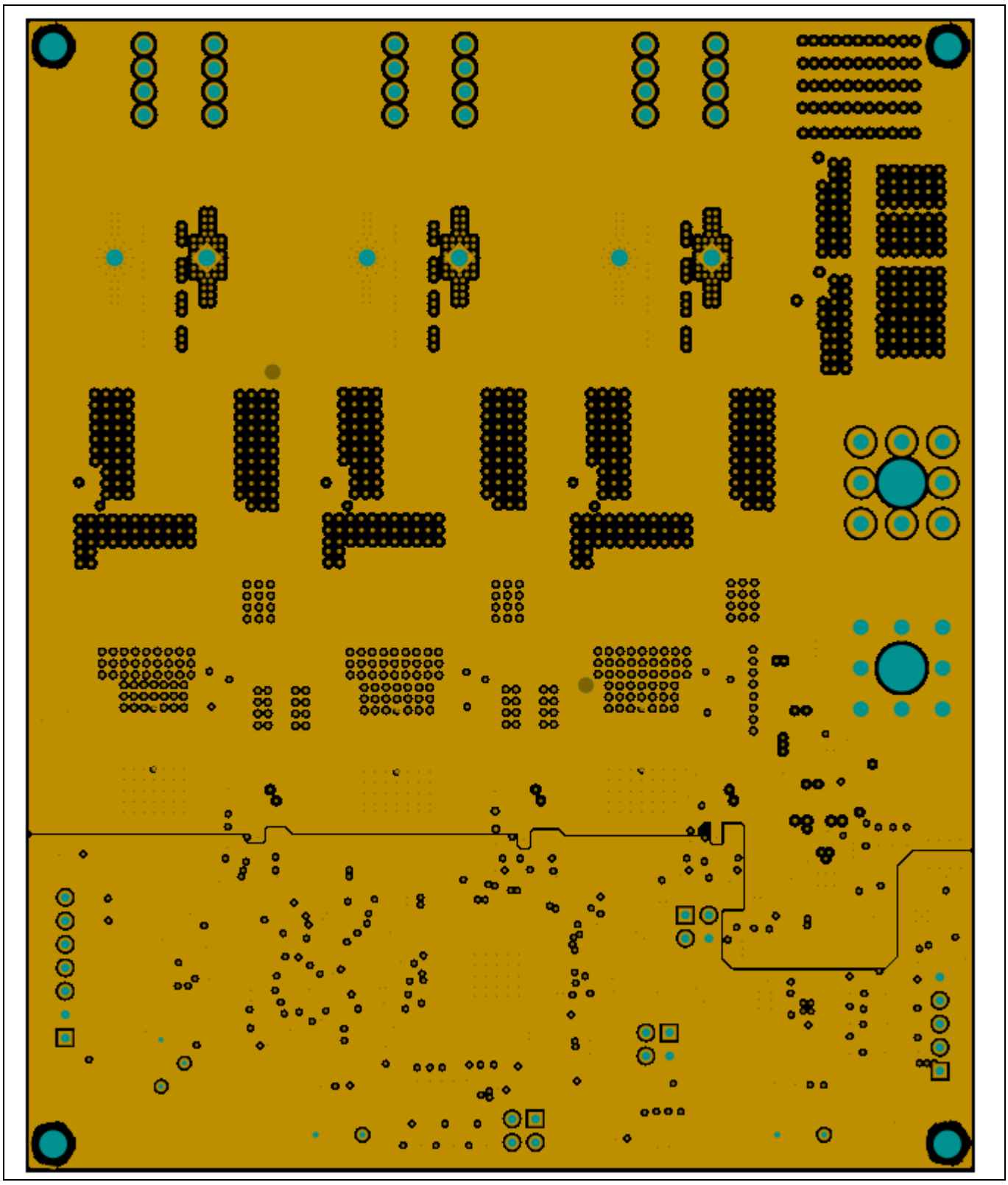

Figure 34 First middle layer

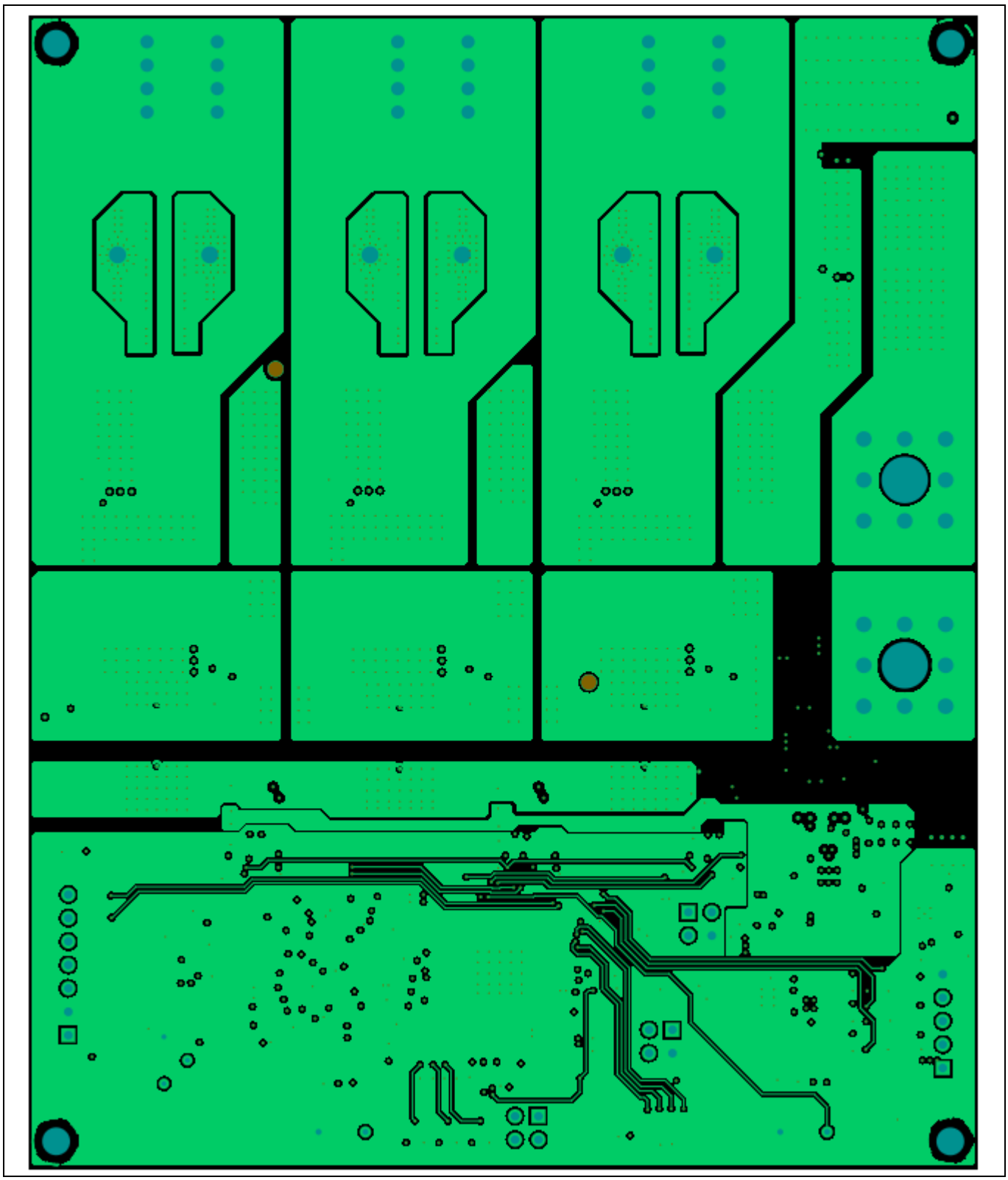

Figure 35 Second middle layer

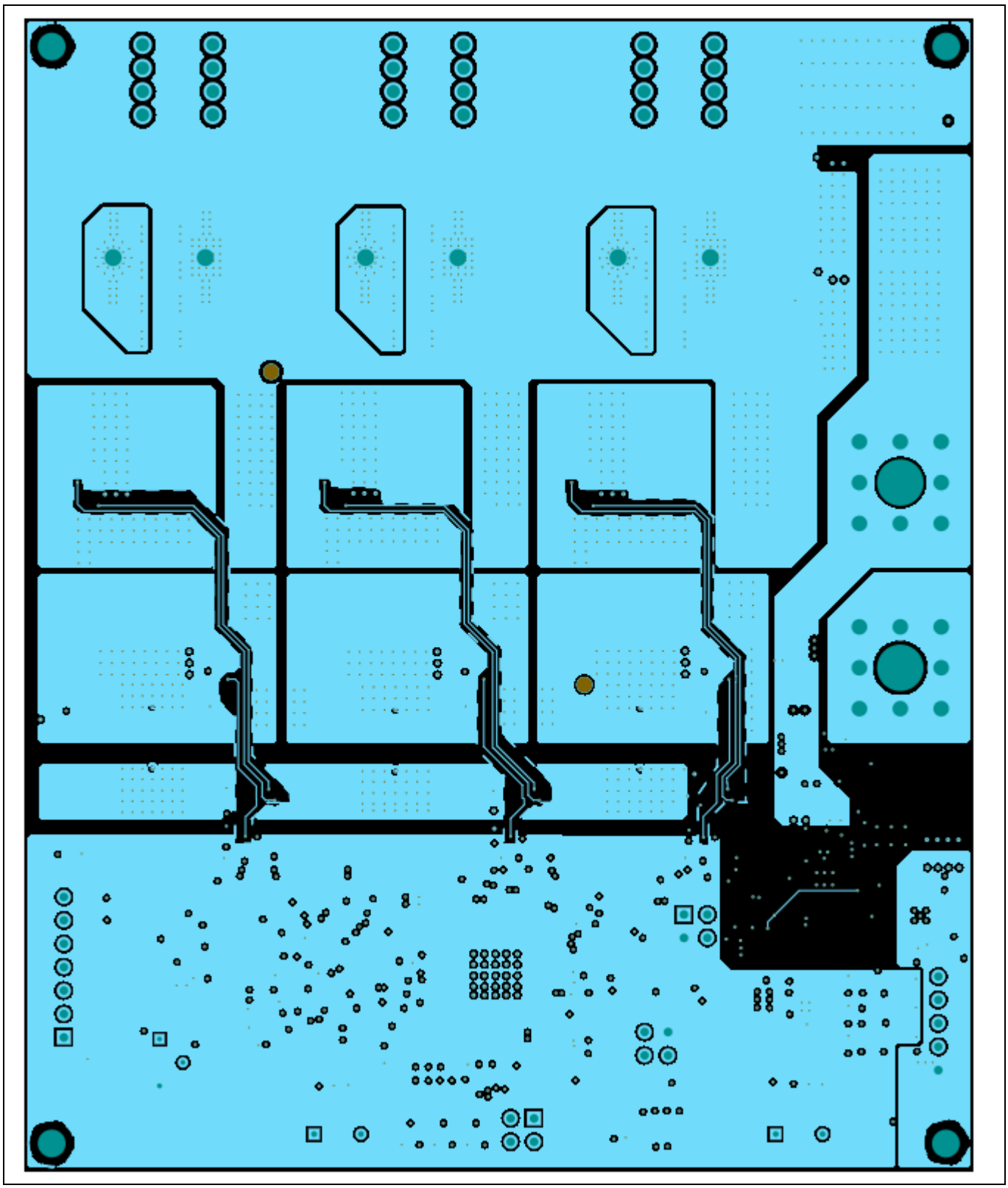

Figure 36 Third middle layer

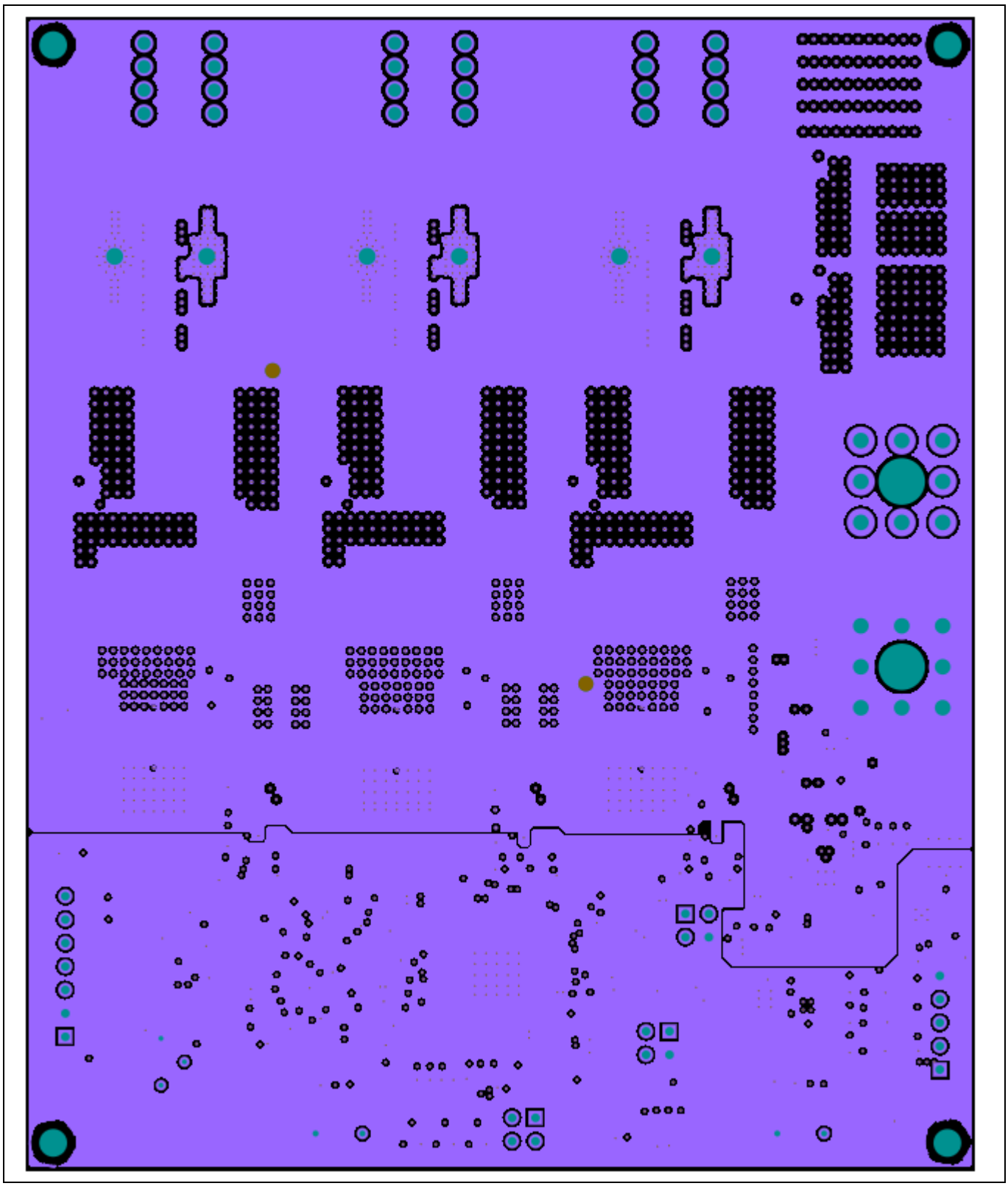

Figure 37 Fourth middle layer

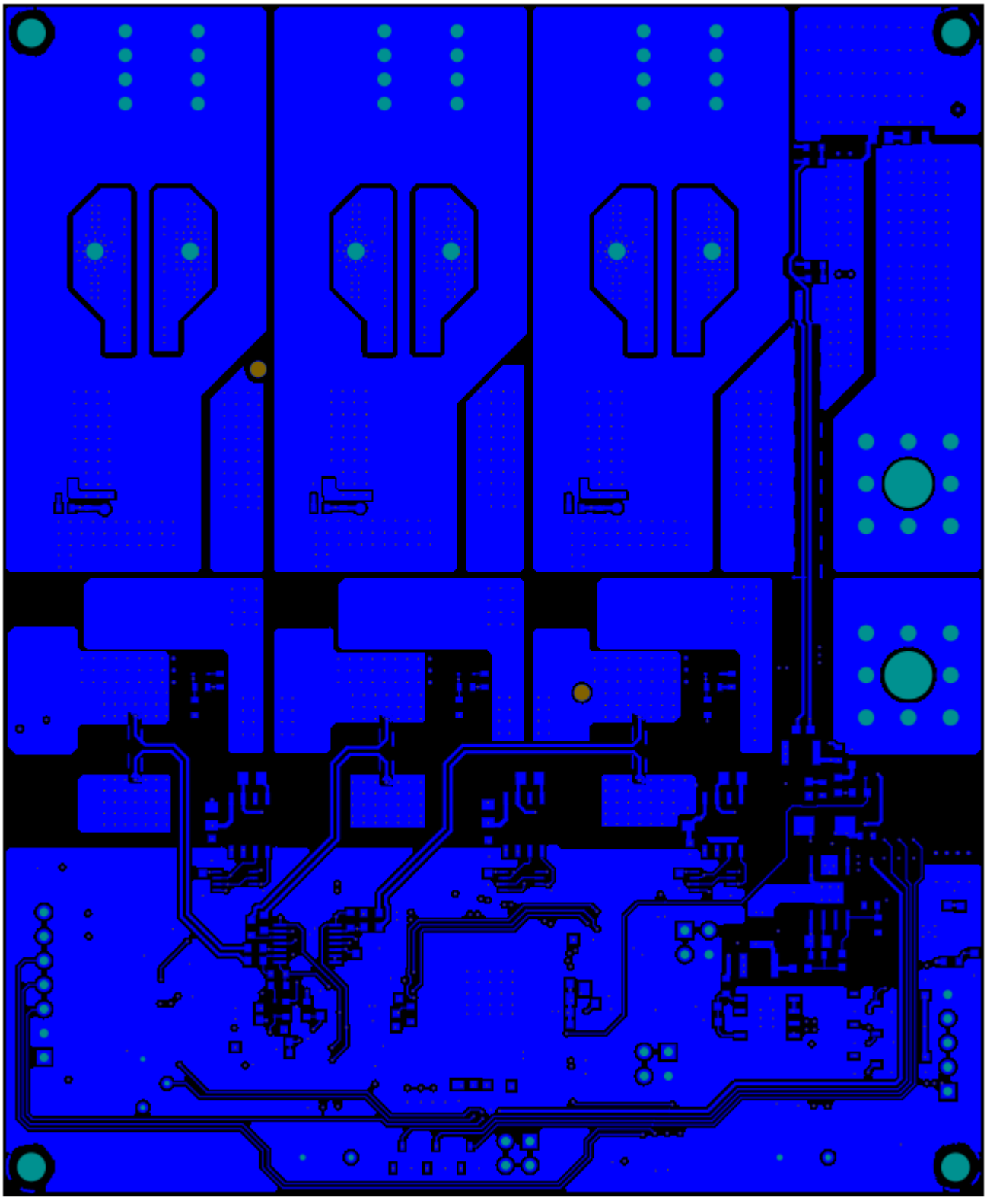

Figure 38 Bottom layer

10 Test results

10.1 Power measurements

Figure 39 shows the captured power measurements while 3.4 Nm of torque was being applied to the motor. The amount of torque being applied prevented the motor from running no more than one minute.

- The first column to the very left shows the DC input voltage (79.540 V) and the V_{rms} measured values of each phase
- The second column shows the measured rms current values for each of the phase and the DC input current (45.031 A)
- The third column shows the output power of the inverter (3.5157 kW) and the column to the very right displays the efficiency

The input power is measured to be $79.540\ \text{V} \times 45.031\ \text{A} = 3.58170\ \text{kW}$,

which provides an efficiency of $\frac{\mathbf{3.5157\ kW}}{\mathbf{3.58170\ kW}} = 98.158\%$.

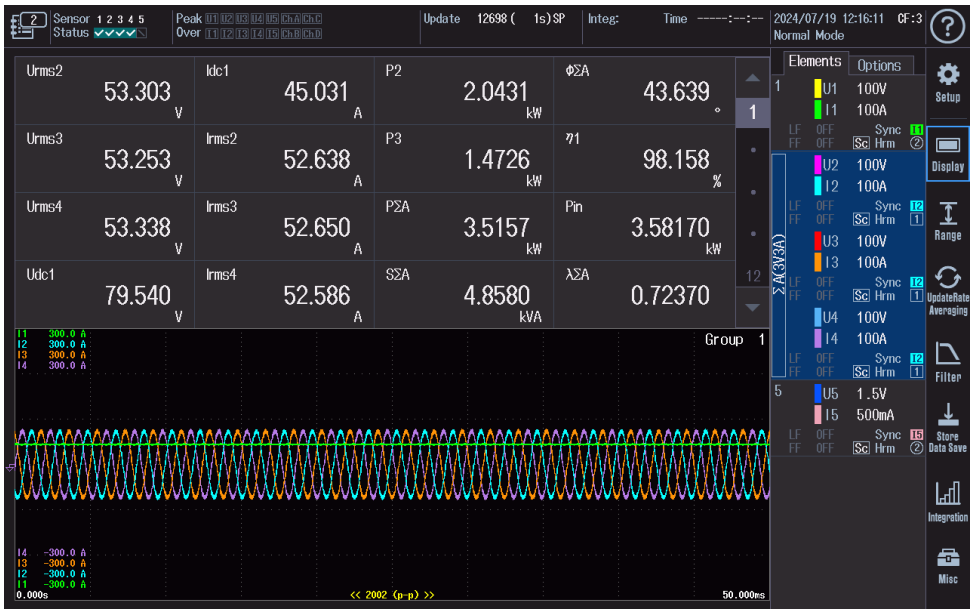

Figure 39 Inverter efficiency (non-continuous)

Figure 40 shows the captured power measurements while 2.6 Nm of torque was being applied to the motor. In this case, the motor was able to run continuously due to a lower torque setting.

- The first column to the very left shows the DC input voltage (79.666 V) and the V_{rms} measured values
- The second column shows the measured rms current values for each of the phase and the DC input current (33.304 A)
- The third column shows the output power of the inverter (2.6107 kW) and the column to the very right displays the efficiency

Input Power is measured to be $3.58170\ \text{kW}$ $(79.540\ \text{V} \times 45.031\ \text{A})$ which provides an efficiency of 98.158%.

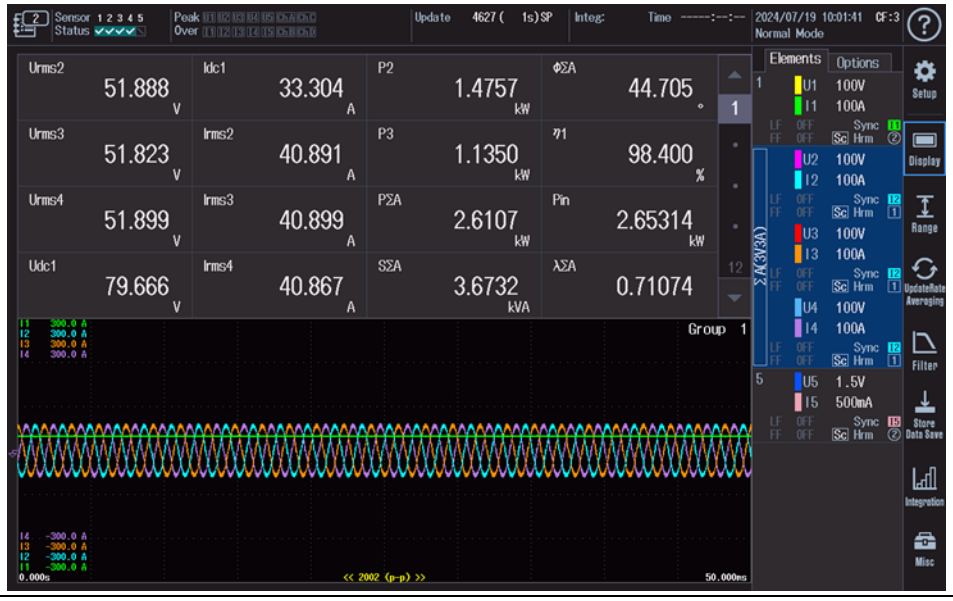

Figure 40 Inverter efficiency (continuous)

10.2 Thermal measurements

Thermal images were taken after 15 minutes of operation to allow the component temperatures to rise and reach steady-state. The motor was running continuously at 8000 rpm at a torque of 2.6 Nm. The thermal camera captured the image in such a way that the cursor would automatically pinpoint the area of the board that had the highest temperature. In both cases, the shunt on the V_{phase} was the component with the highest temperature. The shunt on the V_{phase} had a higher temperature than the other shunts due to a higher amount of current being sensed. The shunts reached a maximum of 87.1°C and a minimum of 86.3°C during testing. The MOSFET's temperature could not be directly monitored due to the heatsink.

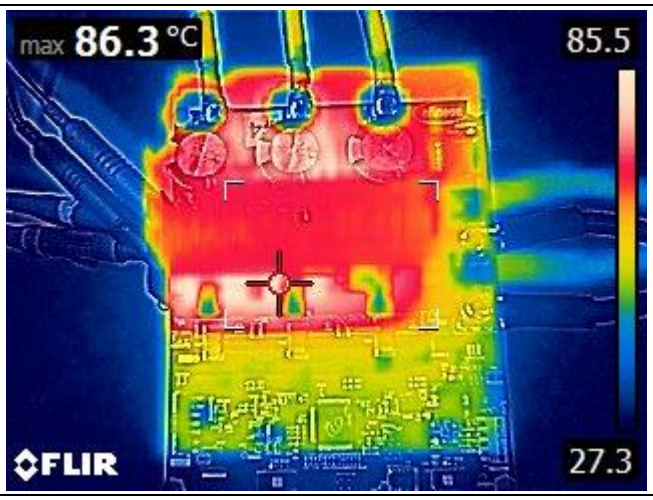

Figure 41 Thermal measurement, 86.3°C

Figure 42 Thermal measurement, 87.1°C

Note: The shunt's reflection on the thermal camera shifted the image upward, giving the illusion that the source of the low-side MOSFET on V_{phase} is the hottest part of the board.

10.3 Operating waveforms

The following waveforms show the currents of each phase as well as V_{DS} (high-side and low-side MOSFETs) from the U phase. The waveforms were captured while driving a motor continuously at 4000 rpm. 2.6 Nm of torque was applied and resulted in 2.6 kW of output power. The switch cycles were captured on the U phase to show the worst-case scenario. Although the U phase is the furthest phase from the battery terminals, the three-phase current waveforms are balanced and the speed is controlled. Figure 44 shows the V_{DS} signals when I_{phase_U} is at its peak. V_{DS_LS} reached a maximum of 93.6 V and remained more than 20% under the MOSFET voltage rating.

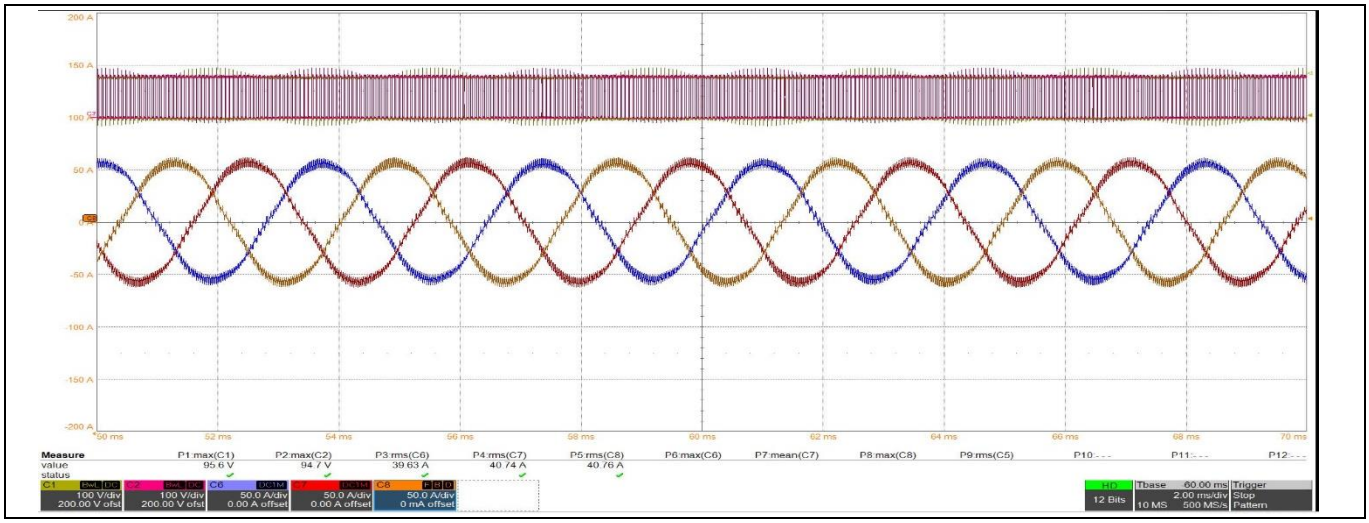

Figure 43 Phase currents and U phase V_{DS} waveforms, 2.6 N·m $V_{DS\_HS\_phU}$ (Ch1), $V_{DS\_LS\_phU}$ (Ch2), I_{phase_U} (Ch6), I_{phase_V} (Ch7), I_{phase_W} (Ch8)

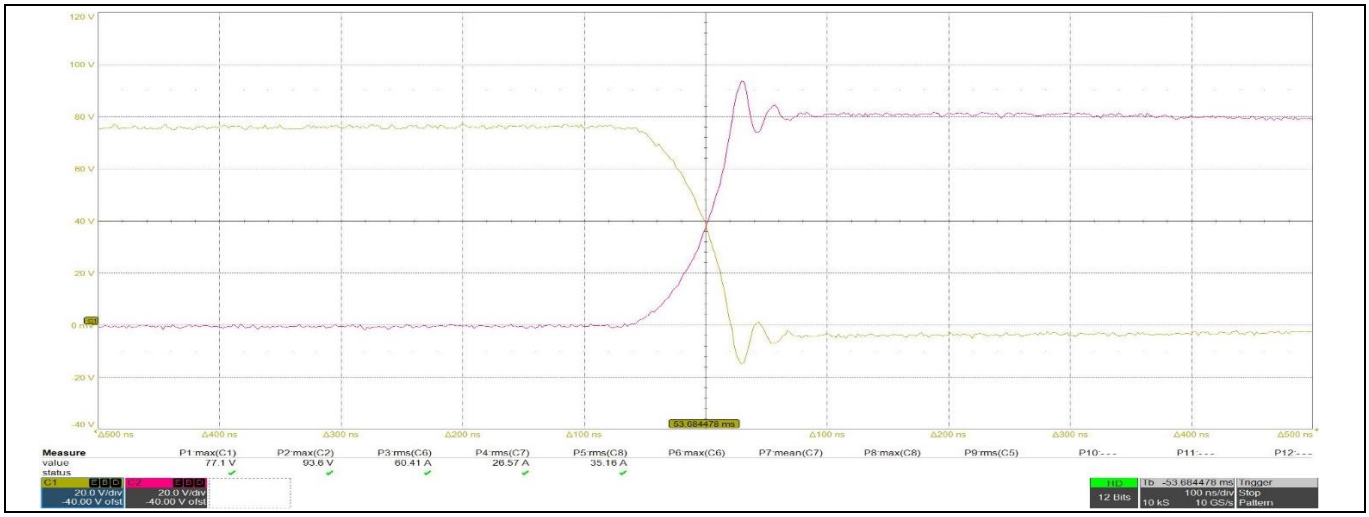

Figure 44 Phase currents and U phase V_{DS} waveforms, 2.6 N·m $V_{DS\_HS\_phU}$ (Ch1), $V_{DS\_LS\_phU}$ (Ch2) (put arrow indicating pk V)

The speed of the motor was increased to 8000 rpm in the figures below (Figure 45 and Figure 46). Although the speed was increased, the current waveforms remained balanced and controlled. Figure 46 shows the V_{DS} signals when I_{phase_U} is at its peak. V_{DS_LS} reached a maximum of 92.6 V, proving that the MOSFETs operate in a suitable safety margin.

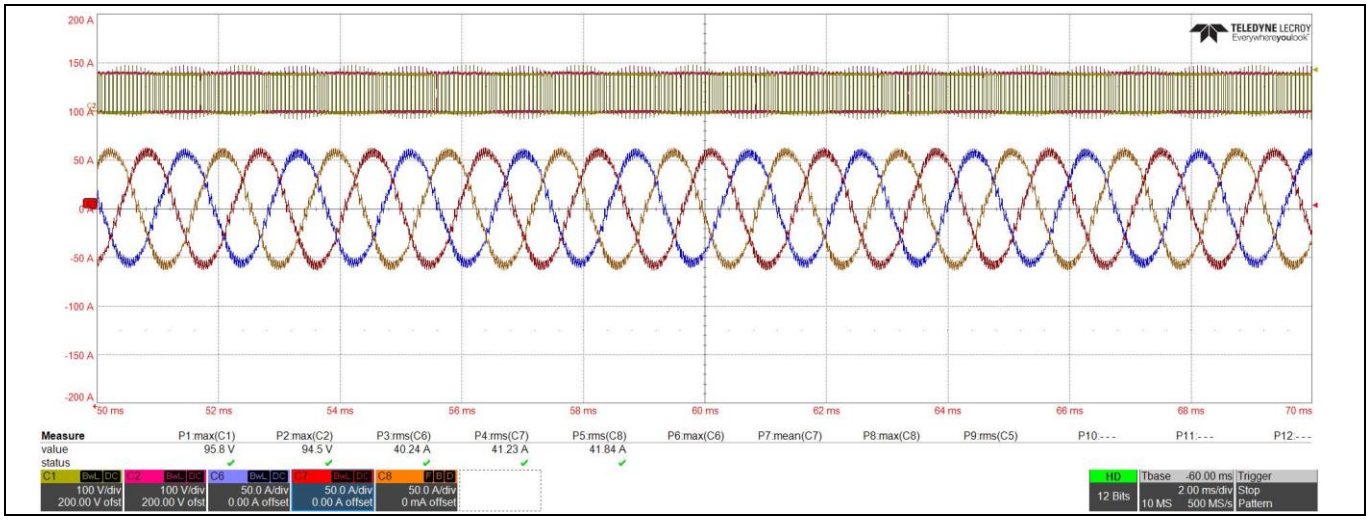

Figure 45 Phase currents and U phase V_{DS} waveforms, 2.6 N·m $V_{DS\_HS\_phU}$ (Ch1), $V_{DS\_LS\_phU}$ (Ch2), I_{phase_U} (Ch6), I_{phase_V} (Ch7), I_{phase_W} (Ch8)

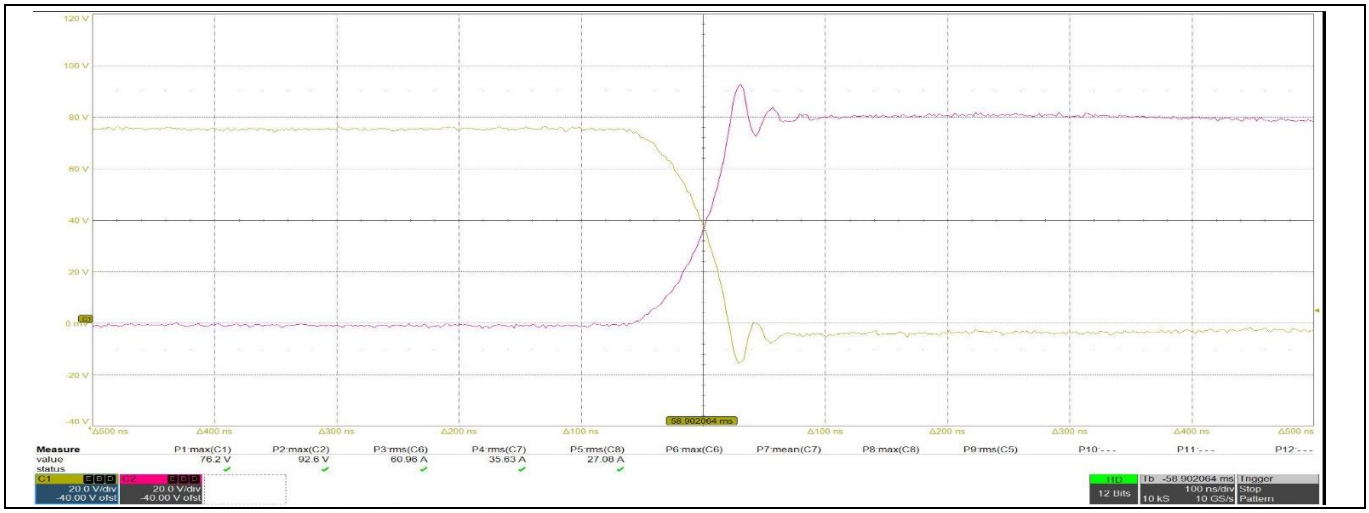

Figure 46 Phase currents and U phase V_{DS} waveforms, 2.6 N·m $V_{DS\_HS\_phU}$ (Ch1), $V_{DS\_LS\_phU}$ (Ch2)

In the figures below, 3.4 N·m of torque was applied and increased the output power to 3.5 kW. Due to the amount of power being drawn, the board was not able to run continuously but still maintained balanced current waveforms (Figure 47 and Figure 48). The high-side and low-side switching signals at 3.5 kW output power (Figure 49). V_{DS_LS} reached a maximum of 96.7 V.

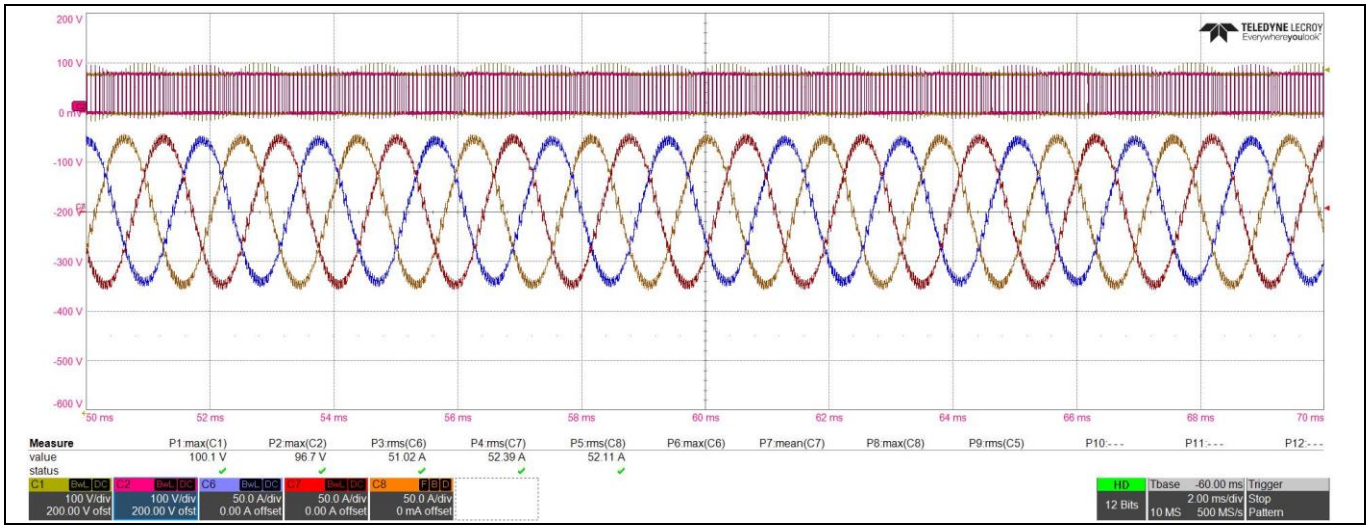

Figure 47 Phase currents and U phase V_{DS} waveforms, 3.4 N·m $V_{DS\_HS\_phU}$ (Ch1), $V_{DS\_LS\_phU}$ (Ch2), I_{phase_U} (Ch6), I_{phase_V} (Ch7), I_{phase_W} (Ch8)

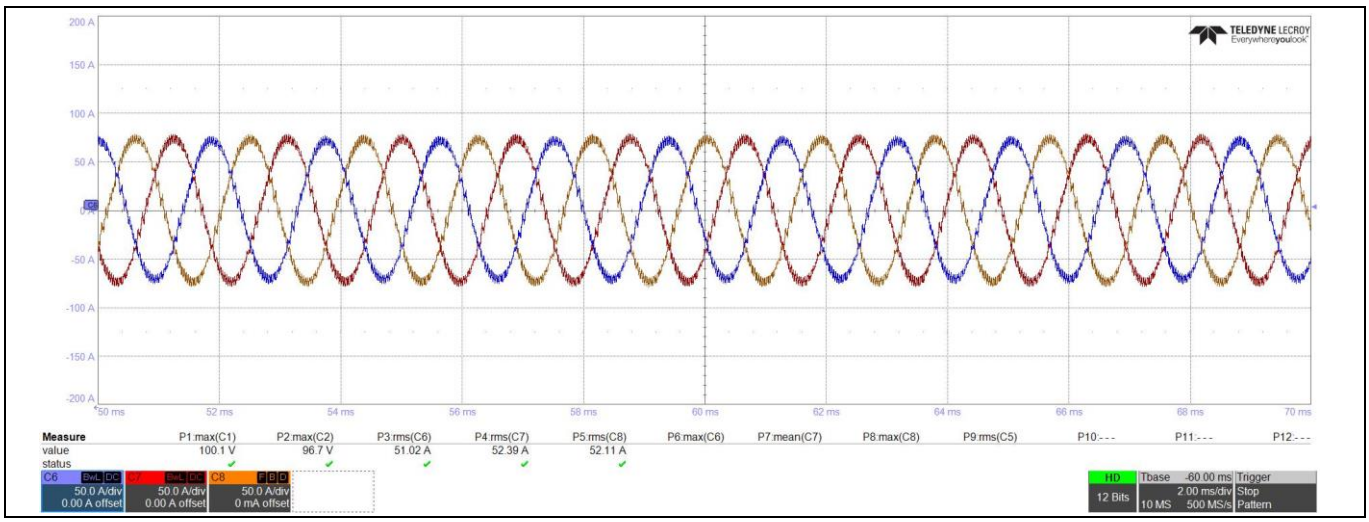

Figure 48 Phase currents, 3.4 N·m I_{phase_U} (Ch6), I_{phase_V} (Ch7), I_{phase_W} (Ch8)

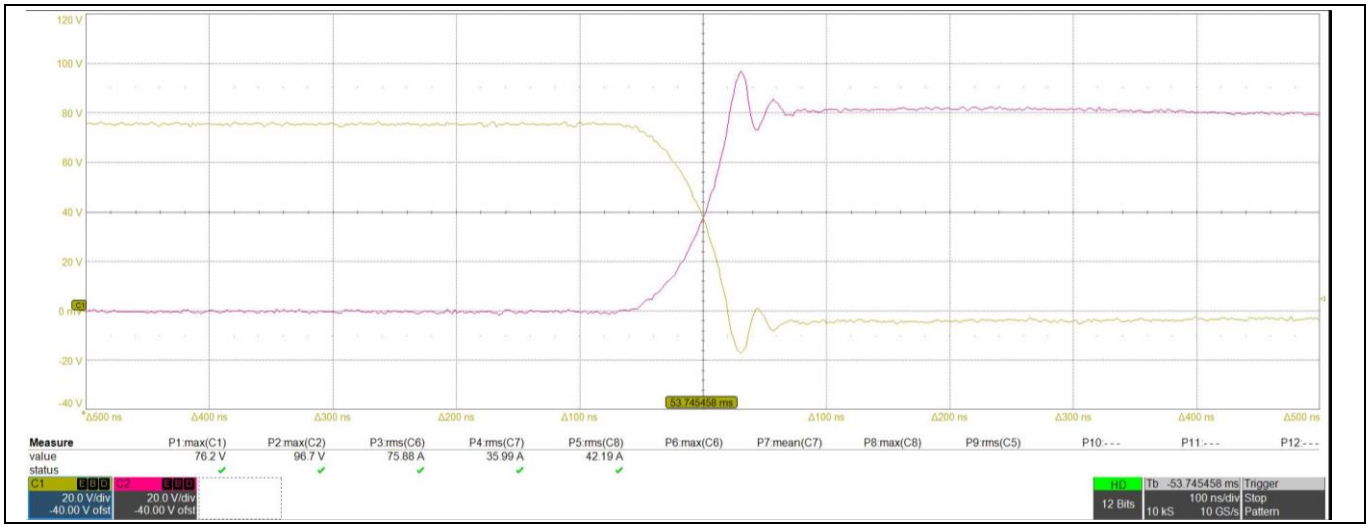

Figure 49 U phase V_{DS} waveforms, 3.4 N·m $V_{DS\_HS\_phU}$ (Ch1), $V_{DS\_LS\_phU}$ (Ch2)

10.4 Electromagnetic compatibility

The board underwent various tests to determine if the electromagnetic energy being emitted is within the FCC 15.109 (g):2024 standards. The board was placed in an anechoic chamber that absorbs the electromagnetic signals. Those signals were then measured by equipment connected to the chamber. The goal was to obtain an emission rate under 37 dBµV/m while the board was in an idle state. The test was conducted at various frequencies ranging from 32 MHz to 999 MHz. No torque was applied and the motor ran at low speed to prevent the motor from overheating. A 48 V power supply with ferrite cores were used in place of a battery. The ferrite cores were snapped onto the power cable to prevent any electromagnetic interference that would not be present in a battery with short terminal wires.

Test results

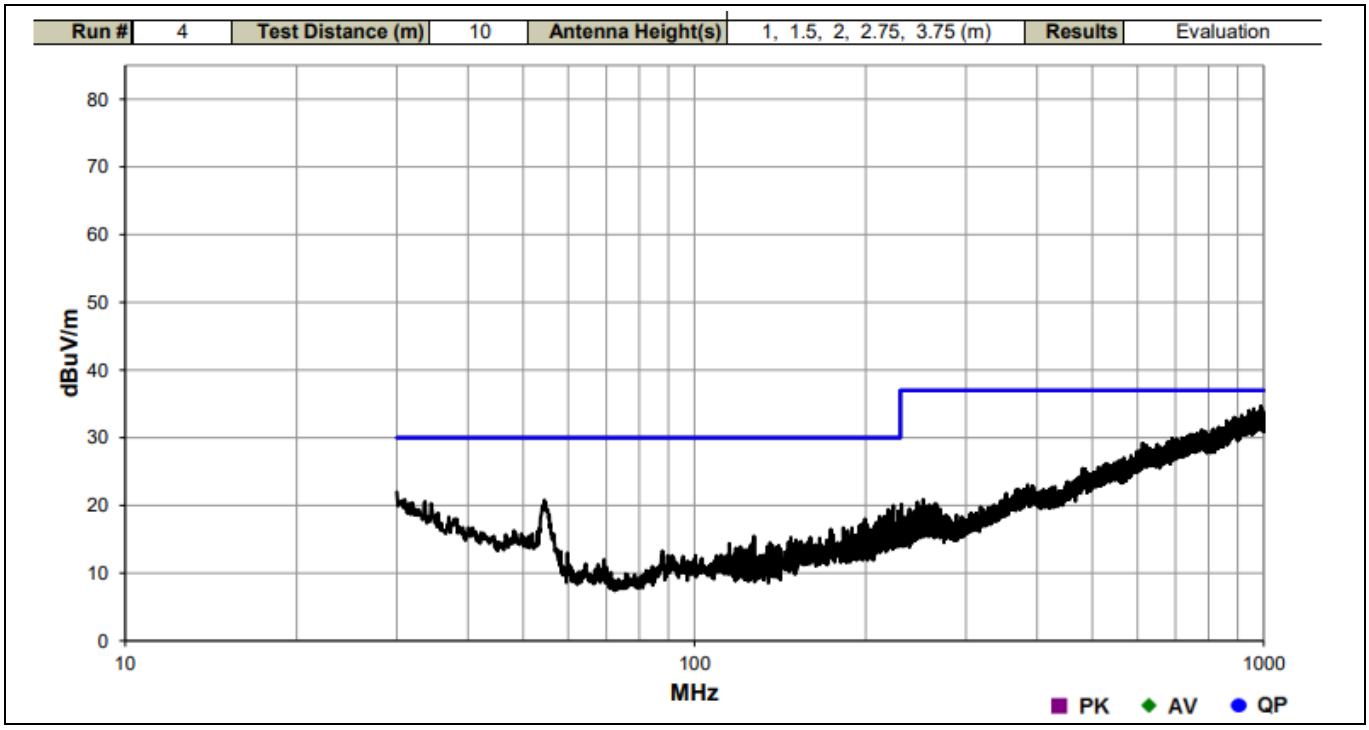

Figure 50 Radiated emission graph

Freq (MHz)	Amplitude (dBuV)	Preamp (dB)	Antenna Height (meters)	Transducer (dB/m)	Cable (dB)	External Attenuation (dB)	Polarity/ Transducer Type	Detector	Distance Adjustment (dB)	Adjusted (dBuV/m)	Spec. Limit (dBuV/m)	Compared to Spec. (dB)
987.754	37.9	42.1	1.0	29.9	8.9	0.0	Horz	PK	0.0	34.6	37.0	-2.4
960.958	38.1	42.3	3.8	29.7	8.8	0.0	Vert	PK	0.0	34.3	37.0	-2.7
942.649	38.1	42.5	2.8	29.8	8.6	0.0	Vert	PK	0.0	34.0	37.0	-3.0
995.271	36.8	42.0	3.8	30.0	9.0	0.0	Vert	PK	0.0	33.8	37.0	-3.2
958.290	37.5	42.3	1.5	29.8	8.7	0.0	Vert	PK	0.0	33.7	37.0	-3.3
961.321	37.5	42.3	2.8	29.7	8.8	0.0	Vert	PK	0.0	33.7	37.0	-3.3
946.529	37.4	42.4	2.8	29.9	8.7	0.0	Horz	PK	0.0	33.6	37.0	-3.4
914.761	37.9	42.6	1.5	29.6	8.4	0.0	Horz	PK	0.0	33.3	37.0	-3.7
936.950	37.4	42.5	2.0	29.6	8.6	0.0	Vert	PK	0.0	33.1	37.0	-3.9
917.186	37.5	42.6	1.0	29.6	8.5	0.0	Horz	PK	0.0	33.0	37.0	-4.0
888.086	37.6	42.6	1.0	29.7	8.3	0.0	Vert	PK	0.0	33.0	37.0	-4.0
932.343	37.5	42.6	2.8	29.5	8.6	0.0	Vert	PK	0.0	33.0	37.0	-4.0
889.541	37.5	42.6	3.8	29.7	8.3	0.0	Horz	PK	0.0	32.9	37.0	-4.1
904.213	37.4	42.6	2.0	29.6	8.4	0.0	Vert	PK	0.0	32.8	37.0	-4.2
900.454	37.3	42.6	3.8	29.7	8.3	0.0	Vert	PK	0.0	32.7	37.0	-4.3
860.805	37.9	42.5	2.0	29.0	8.1	0.0	Horz	PK	0.0	32.5	37.0	-4.5
834.373	37.6	42.5	1.0	28.6	7.9	0.0	Horz	PK	0.0	31.6	37.0	-5.4
846.861	37.2	42.5	1.0	28.7	8.0	0.0	Horz	PK	0.0	31.4	37.0	-5.6
816.913	37.7	42.4	3.8	28.2	7.8	0.0	Vert	PK	0.0	31.3	37.0	-5.7
777.628	37.3	42.2	3.8	28.4	7.6	0.0	Horz	PK	0.0	31.1	37.0	-5.9

Figure 51 Radiated emission table

11 Summary

The REF_80VDC_3.5KW_OPE2 reference board meets specifications. The principle of operation, design of the circuitry, control scheme, and PCB layout have all been discussed. The option for motor speed, direction, and braking can be controlled locally with switches and a potentiometer located on the board. In addition, the motor speed, direction, and braking can be controlled via a GUI.

The GUI provides different FOC options which allow easy customization of firmware parameters. The GUI has also been proven to be a useful tool for motor tuning. The ability to install customized firmware and configuration parameters to the system greatly simplifies the design process, eliminates unnecessary components, and is thereby able to simplify product development and reduce time-to-market.

The firmware has been verified through testing. The FOC control algorithm has also been described, including the methods for entering the motor parameters and tuning the control loops using ModusToolbox™. The test results show that Andromeda is effective in important areas such as speed control, phase advance, MPTA, flux weakening, MTPV, and current controlling. Mathematical models have been shown and used to explain how andromeda is implemented. The equations and algorithms for these areas have been explained in this application note.

Test results show that the REF_80VDC_3.5KW_OPE2 reference board operates with better than 98% efficiency while driving a 3.5 kW load with a temperature rise of less than 45°C on the power device packages in the open air with convection cooling. The reference board can support 3.5 kW with no additional cooling and can operate at a steady state at 2.5 kW for 15 minutes while maintaining a temperature lower than 90°C. Despite the waveforms being captured on the U phase showing the worst-case scenario, the current waveforms were balanced with little ripple through high-speed testing (8000 rpm), low-speed testing (4000 rpm), high torque testing (3.4 N·m), and low torque testing (2.6 N·m). The EMI test results show that the reference board operates within all major market regulations including the FCC 15.1 109 (g):2024 standards. The board is able to function properly at high frequencies while remaining under the emission limit of 37 dBuV/m.

References

[1] Infineon Technologies AG: *Motor Handbook (Version 2.1)*; Available online

[2] Infineon Technologies AG: *Sensorless Field Oriented Control with Embedded Power SoC*; Available online

[3] Infineon Technologies AG: *Application note - Block commutation vs. FOC in power tool motor control*; Available online

[4] Infineon Technologies AG: *Application note - PMSM FOC motor control software using XMC™*; Available online

[5] Infineon Technologies AG: *Whitepaper - Power Loss and Optimized MOSFET Selection in BLDC Motor Inverter Designs – Understanding MOSFET power losses in block (trapezoidal) commutation*; Available online

[6] Zhang, Wei-Feng Zhang/Yu, Yue-Hui: *Comparison of Three SVPWM Strategies*; Journal of Electronic Science and Technology of China (Vol. 5, No. 3); 2007-09

[7] Magtrol: *Hdseries - Hysteresis Dynamometers - HD Series*, 2023; Available online

[8] Infineon Technologies AG: Behjati, Hamid, et al: *Motor Control Firmware Reference Manual*; May 1, 2024

Register your Infineon evaluation board, reference design, or demo kit board

When receiving your order, you are only three steps away from unlocking what our application engineers have prepared for you, as the new owner of a very specific Infineon evaluation board, reference design or demo kit: Product registration

Revision history

Document revision	Date	Description of changes
V 1.0	2025.01.28	Initial release

Trademarks

All referenced product or service names and trademarks are the property of their respective owners.

PSOC™, formerly known as PSoC™, is a trademark of Infineon Technologies. Any references to PSoC™ in this document or others shall be deemed to refer to PSOC™.

Edition 2025-01-28

Published by

Infineon Technologies AG

81726 Munich, Germany

Do you have a question about this document?

Email: erratum@infineon.com

Document reference

AN024149

Important notice

The information contained in this application note is given as a hint for the implementation of the product only and shall in no event be regarded as a description or warranty of a certain functionality, condition or quality of the product. Before implementation of the product, the recipient of this application note must verify any function and other technical information given herein in the real application. Infineon Technologies hereby disclaims any and all warranties and liabilities of any kind (including without limitation warranties of non-infringement of intellectual property rights of any third party) with respect to any and all information given in this application note.

The data contained in this document is exclusively intended for technically trained staff. It is the responsibility of customer's technical departments to evaluate the suitability of the product for the intended application and the completeness of the product information given in this document with respect to such application.

Warnings

Due to technical requirements products may contain dangerous substances. For information on the types in question please contact your nearest Infineon Technologies office.

Except as otherwise explicitly approved by Infineon Technologies in a written document signed by authorized representatives of Infineon Technologies, Infineon Technologies' products may not be used in any applications where a failure of the product or any consequences of the use thereof can reasonably be expected to result in personal injury.